SLL-I
CL

HIGH PRESSURE CW CHEMICAL LASER

AO 1180

SLL 82-244/CL-I

David Rensch

Hughes Research Laboratories
3011 Malibu Canyon Road
Malibu, CA 90265

November 1976

Contract DAAH01–75–C–0412
Final Technical Report – Phase I
For Period 15 August 1975 to 22 June 1976

The views and conclusions contained in this document are those of the authors and should not be interpreted as necessarily representing the official policies, either expressed or implied, of the Defense Advanced Research Projects Agency or the U.S. Government.

Sponsored By
DEFENSE ADVANCED RESEARCH PROJECTS AGENCY
ARPA Order No. 1180

This research was supported by the Defense Advanced Research Projects Agency of the Department of Defense and was monitored by the U.S. Army Missile Command under Contract Number DAAH01–75–C–0412.

U3893

Accession Number: 3893

Publication Date: Nov 01, 1976

Title: High Pressure CW Chemical Laser

Personal Author: Rensch, D.

Corporate Author Or Publisher: Hughes Research Laboratories, 3011 Malibu Canyon Rd., Malibu, CA 90265

Report Prepared for: U.S. Army Missile Command, Redstone Arsenal, AL 35809

Comments on Document: Archive, RRI, DEW

Descriptors, Keywords: High Pressure Continuous Wave Chemical Laser Hydrogen Fluoride Deuterium Electric Discharge Fluorine Demonstration Subsonic Flow E-beam SustainArgon Mixture

Pages: 00081

Cataloged Date: Nov 27, 1992

Contract Number: DAAH01-75-C-0412

Document Type: HC

Number of Copies In Library: 000001

Record ID: 25221

Source of Document: DEW

UNCLASSIFIED

SECURITY CLASSIFICATION OF THIS PAGE *(When Data Entered)*

REPORT DOCUMENTATION PAGE		READ INSTRUCTIONS BEFORE COMPLETING FORM
1. REPORT NUMBER	2. GOVT ACCESSION NO.	3. RECIPIENT'S CATALOG NUMBER
4. TITLE *(and Subtitle)* HIGH PRESSURE CW CHEMICAL LASER		5. TYPE OF REPORT & PERIOD COVERED Final Tech Report-Phase I 15 Aug. 1975-22 June 1976 6. PERFORMING ORG. REPORT NUMBER
7. AUTHOR(s) David Rensch		8. CONTRACT OR GRANT NUMBER(s) DAAH01-75-C-0412
9. PERFORMING ORGANIZATION NAME AND ADDRESS Hughes Research Laboratories 3011 Malibu Canyon Road Malibu, California 90265		10. PROGRAM ELEMENT, PROJECT, TASK AREA & WORK UNIT NUMBERS ARPA Order No. 1180
11. CONTROLLING OFFICE NAME AND ADDRESS Defense Advanced Research Projects Agency Arlington, Virginia 22209		12. REPORT DATE November, 1976 13. NUMBER OF PAGES 81
14. MONITORING AGENCY NAME & ADDRESS *(if different from Controlling Office)* U.S. Army Missile Command Attn: AMSMI-RNS Restone Arsenal, AL 35809		15. SECURITY CLASS. *(of this report)* UNCLASSIFIED 15a. DECLASSIFICATION DOWNGRADING SCHEDULE
16. DISTRIBUTION STATEMENT *(of this Report)*		
17. DISTRIBUTION STATEMENT *(of the abstract entered in Block 20, if different from Report)*		
18. SUPPLEMENTARY NOTES		
19. KEY WORDS *(Continue on reverse side if necessary and identify by block number)* HF/DF Chemical Laser, Continuous Wave, High Pressure, Electrical Discharge		

20. ABSTRACT *(Continue on reverse side if necessary and identify by block number)*

A fast-flow demonstration device is described which has a channel cross-section of 2.5 cm high by 6 cm long. It was constructed to evaluate the performance of a cw, H_2-F_2-He laser system operating at cavity pressures near one atmosphere and flow Mach numbers between 0.6 and 1.5. A small percentage of the F_2 is dissociated by passing the premixed gas flow through an e-beam sustained electrical discharge. Predictions of laser system performance are presented

DD FORM 1 JAN 73 1473 EDITION OF 1 NOV 65 IS OBSOLETE

UNCLASSIFIED

SECURITY CLASSIFICATION OF THIS PAGE *(When Data Entered)*

and discussed for both supersonic and subsonic flow. Experimental results characterizing the electrical discharge are presented for a wide range of operating parameters. Difficulties encountered in initiating the flowing gas mixture are discussed above with various experiments conducted to determine the cause. The latter experiments point to insufficient fluorine dissociation by the electrical discharge. This conclusion is supported by results presented from a discharge kinetics code.

TABLE OF CONTENTS

LIST OF ILLUSTRATIONS

LIST OF ILLUSTRATIONS (Cont'd)

LIST OF ILLUSTRATIONS (Cont'd)

I. INTRODUCTION

A. Motivation

Present cw combustion-driven chemical lasers operate over a limited range of cavity pressures (typically 5 to 15 Torr). This restriction is caused by the finite mixing length of the gas reactants in the laser cavity. For government service applications, low cavity pressures impose severe penalties on system size and weight if the laser device is going to be operated below altitudes of 10 km. Below this altitude, atmospheric pressure exceeds the capability of supersonic diffusers and additional pumping by ejector pumps is required. Because ejectors require a mass flow rate of 5 to 10 times the mass flow rate of the laser, and because they must operate at high stagnation pressures, the weight of the ejector can exceed thousands of pounds. Under the present contract we plan to overcome these limitations by operating a chemical laser device at near atmsopheric pressure ($\simeq$500 Torr).

The high-pressure cw HF/DF laser device differs from present cw chemical lasers in the method of mixing the chemical reactants and in initiating the chemical reaction. The device mixes the gas reactants and diluent in a high-pressure, subsonic flow region; expands the homogeneous mixture through a nozzle with an exit pressure near atmospheric pressure; and initiates the gas mixture with an electron beam-controlled electrical discharge. By premixing the gas reactants, the present limitation in cavity pressure of 5 to 10 Torr in cw HF/DF lasers is overcome. Considerably higher cavity pressures and laser operation without large pumps to boost the laser exhaust gases to atmospheric pressure are feasible. Our ultimate goal is to develop an efficient cw chemical laser capable of operating at near-atmospheric cavity pressures.

Emphasis of the present work was to acquire data and explanatory analysis as to the advanced technology which may be required for the development of a high-pressure cw HF/DF chemical laser. To this end, we fabricated a small-scale demonstration device. The specific program objectives are described below:

1. Task 1

Perform any preliminary analysis necessary for the successful design and construction of a small-scale experimental laser device.

2. Task 2

Design and construct a fast-flow, cw, high-pressure, HF/DF chemical laser. Included shall be an electron gun, sustainer discharge apparatus, expansion nozzles, flow channels, and reactant feed systems. Design and fabrication of the components shall be optimized with respect to performance, flexibility, and run time.

3. Task 3

Perform measurements to determine the cold-flow gas dynamic properties. Determine the relationship between the gas flow properties and electrical input energy and determine the efficiency of fluorine dissociation versus electrical input energy.

B. Technical Approach

The design of a high-pressure, cw chemical laser must incorporate gas dynamic and thermodynamic effects of fast-flow, HF/DF kinetics, and electrical discharge initiation. Under Task 1 a review was undertaken of the key experimental and theoretical results that bear directly upon our choice of technical approach, and the results are presented in Section II.

Successful operation of an HF/DF cw chemical laser requires two essential elements: (1) a stable, premixed flow of reactants possessing good optical and chemical homogeneity, and (2) an initiation technique which provides a uniform cw electrical discharge having sufficient energy to dissociate a prescribed amount of molecular fluorine. Techniques for achieving the first element have been developed on a previous contract.* Under Task 2 these techniques were extended to the higher pressure and fast gas flow required for the small-scale demonstration device. The design of the device is discussed in Section III. A laser cavity with a height of 2.5 cm and a length in the nozzle direction of 6 cm was selected as being compatible with contract goals, and providing the fast gas flow for 0.5 to 1.0 sec.

The gas flow system utilizes separate storage of $He-H_2$ and $He-F_2$ mixtures, mixes on-the-fly upstream of the nozzle, expands the gas flow to Mach number M = 0.6 to 1.5, and exhausts into a 90 ft^3 dump tank. This system provides choice of operating pressure from <100 Torr to 500 Torr.

To achieve the second element, an electrical discharge is provided by a 26-μF capacitor bank (maximum charge voltage is 25 kV) connected to the discharge electrodes via a high-voltage vacuum relay. Conditioning of the discharge volume is accomplished by irradiation from a plasma cathode electron gun. The discharge electrodes consist of a resistive anode (polyester and carbon mixture) shaped in a plano-elliptic configuration and the foil window of the e-gun acts as the cathode. Both electrodes are flush mounted in the top and bottom walls of the cavity to prevent gas flow disturbances.

The experimental program consisted of gas flow diagnostics and electrical discharge measurements. The details of these measurements are presented in Section IV. Briefly, extensive electrode voltage and current characteristics were obtained for cavity pressures between 100 and 400 Torr, gas mixtures containing F_2 concentrations

*"Chemical Laser Pulse Initiation Study," F29601-72-C-0007.

between 3 and 10 percent, e-beam current densities between 0 and 0.5 mA/cm^2, and gas flow Mach numbers between 0.6 and 1.5. No combination of the above parameters succeeded in initiating an observable chemical reaction. Four possibilities are presented to explain the lack of any chemical reaction, along with the results from several experiments which eliminate three of the four. The fourth possibility is discussed more fully in Section V, where the results from a computer code used to analyze fluorine dissociation in e-beam electrical discharges are presented. These results strongly indicate that low e-beam current densities, such as the type required for cw devices, are ineffective in dissociating F_2 in e-beam sustained discharges.

Based upon the results discussed in this report, program efforts directed toward the development of a high-pressure cw chemical laser have been terminated. A program redirection has been completed which will continue to emphasize high-pressure chemical lasers, but on a repetitively pulsed basis rather than cw.

II. TECHNICAL BACKGROUND

A. Introduction

This section provides a review of the key experimental and theoretical results that bear directly upon our choice of technical approach for a high-pressure cw chemical laser. The three technical subjects discussed in Section B are gas dynamics and thermodynamics, HF/DF and DF/CO_2 kinetics, and initiation.

B. High-Pressure CW Chemical Laser

1. Gas Dynamics and Thermodynamics

The high-pressure cw chemical laser requires near-sonic flow to give reasonable lasing lengths and efficient laser operation. At 500 Torr, the lasing time for a F_2:H_2:He mixture at 1:1:30 is approximately 60 μsec for an initial fluorine dissociation of only 0.25%. For supersonic flow velocities of 1×10^5 cm/sec (this corresponds to a Mach number M = 1.5 at a gas temperature T = 175°K), the lasing zone is approximately 4 cm in the flow direction. Decreasing the flow velocity below this value requires the fluorine dissociation percentage to decrease below 0.25 to prevent shrinking of the lasing zone. Since small fluorine dissociations are detrimental to obtaining high electrical and chemical efficiency, flow velocities must approach sonic velocities to maintain fluorine dissociation levels large enough for efficient laser operation.

An important difference between the present supersonic cw chemical lasers and the high-pressure laser is the amount of heat released into the optical cavity. Because present cw chemical lasers operate using the less energetic "cold" reaction, while the high-pressure device uses the full chain reaction, considerably more heat is released by the latter. For initial Mach numbers near M = 1.5 in

the high-pressure devices, the flow will become subsonic as a result of the heat input at some downstream location before exhausting to the atmosphere.

To obtain insight into the flow properties with heat input, we used the one-dimensional, continuous flow analysis of Shapiro.[1] The initial conditions imposed by chemistry are (1) the plenum temperature must be 300°K to avoid prereaction, (2) the supersonic expansion is limited to $M < 2.5$ to avoid condensation of the F_2 and low laser efficiency, and (3) the cavity pressure must be ≃1.0 atm. The following flow modes were considered:

1. Constant static pressure
2. Constant Mach number M
3. Constant temperature T.

Both constant M and constant T operation involve very large static pressure drops through the reaction zone. The resulting loss in stagnation pressure is also large. Operation at constant static pressure also produces a decrease in stagnation pressure, but much less than with the other two cases.

Variation in initial Mach number has the surprising effect of reducing the stagnation pressure as the initial Mach number is increased. This is a direct result of the low temperatures which occur in the flow at high Mach numbers, since entropy generation, which is proportional to dQ/T, is greater at lower temperatures. The usual technique for eliminating this problem (i.e., heating the plenum) cannot be utilized here for the reasons explained above. The best compromise between high velocity and minimum pressure loss appears to be $M \simeq 1.5$.

For a gas mixture with constant specific heat and molecular weight, the differential equations for Mach number M and pressure P are

$$\frac{dM^2}{M^2} = -\left[\frac{1 + \frac{\gamma - 1}{2} M^2}{1 - M^2}\right]\left[-\frac{2dA}{A} + (1 + \gamma M^2)\frac{dT_o}{T_o}\right] \tag{1a}$$

$$\frac{dP}{P} = \frac{\gamma M^2}{1 - M^2}\left[\frac{dA}{A} - \left(1 + \frac{\gamma - 1}{2} M^2\right)\frac{dT_o}{T_o}\right] \tag{1b}$$

where A, T_o, and γ are the flow area, total temperature, and ratio of specific heats, respectively. For constant velocity flow

$$dT = \frac{dQ}{C_p} \tag{2a}$$

$$\frac{dM^2}{M^2} = -\frac{dT}{T} \tag{2b}$$

$$\frac{dT_o}{T_o} = \frac{dQ}{C_p T}\left(\frac{1}{1 + \frac{\gamma - 1}{2} M^2}\right) \tag{2c}$$

where Q, C_p, and T are the heat addition due to the reaction, the specific heat at constant pressure, and the local gas temperature. Rewriting eqs. (1) and (2), we find that

$$\frac{dA}{A} = \frac{dT}{T} \quad , \text{and} \quad \frac{dP}{P} = 0 \tag{3}$$

The results of eq. (3) state that if the flow area expands proportionally with temperature T, the flow maintains constant pressure and velocity. Using eq. (3) to rewrite eq. (1), we can solve for M in terms of T_o

$$\frac{dM^2}{M^2} = -\left(1 + \frac{\gamma - 1}{2} M^2\right)\frac{dT_o}{T_o} \tag{4}$$

It can be seen that the Mach number decreases monotically with the increasing total temperature T_o or heat addition. In contrast to eq. (1), eq. (4) exhibits no singularity at M = 1. Therefore, in theory, the flow can pass from supersonic to subsonic flow at some point downstream in the channel without choking. Rapid increases in flow area will definitely cause some two-dimensional effects, resulting in lower pressure near the channel walls. Since the rate of expansion of the channel increases as the height of the channel entrance is increased, two-dimensional effects will definitely place a limit on device scaling in this direction. The expansion rate for the small-scale demonstration device, however, is expected to be smaller than the expansion rate used for its supersonic nozzles. We verified this assumption by using a one-dimensional nozzle program[2] to calculate the pressure and temperature downstream of the discharge region for a F_2:H_2:He mixture of 1:1:30, cavity pressure of 500 Torr, $F/2F_2$ dissociation percentage of 0.3%, initial flow Mach number M = 1.5, and linear divergent top and bottom cavity channel walls. The calculations assumed one-dimensional flow (no transverse pressure gradients) and were terminated when $M \rightarrow 1$. The results showed that for divergence half angles greater than ~3° the cooling effect of the supersonic expansion quenched the chemical reaction. For these expansion rates the temperature and pressure decreased in the downstream direction. For angles between 2 and 3°, the pressure remained nearly constant while temperature and the chemical reaction rate increased.

2. HF/DF and DF-CO_2 Kinetics

In our analysis of high-pressure cw chemical lasers we used a laser kinetics computer program that consists of three interacting subprograms to treat dissociation, reaction kinetics, and laser action. Both our HF and DF-CO_2 kinetics programs have been extensively checked against experimental data obtained on electrically pulsed and flash-photolysis-premixed chemical lasers at Hughes Research Laboratories (HRL). Initial checks of the HF program showed the

predicted laser power and pulse length to be too large. To bring the predicted and experimental results closer together, we changed from a linear vibrational-level dependence V on the HF vibrational-translational V-T relaxation rate to a quadratic dependence V^2. While this change brought the two results closer, the HF kinetics model still predicted too much energy. Although we found that we could get good agreement by increasing the HF(1) V-T relaxation rate, we do not have additional justification for the increase.

In Fig. 1 we have compared the measured output power from HRL's 10-liter flash-photolysis HF/DF chemical laser[3] with the calculated results from our HF/DF kinetics program. For the comparison we used F_2:H_2:He = 1.5:1:15, cavity pressure = 200 Torr, and fluorine dissociation $F/2F_2$ = 0.02%. The fluorine dissociation level for the modeling was determined by first operating the laser as a DF-CO_2 laser. Since the power output from the DF-CO_2 laser is relatively insensitive to V-T deactivation of DF, accurate modeling of the laser's power output, pulse length, and turn-on time can be made by using only one variable — fluorine dissociation. The results in the figure were obtained using an HF(1) V-T relaxation rate of $\tau_{HF}P(HF)$ = 0.0085 μsec-atm. It can be seen that the calculated pulse turn-on time, pulse length, and output power are in good agreement with the measured results.

The computer programs, although originally developed for analysis of pulsed lasers, can be extended to our high-pressure device because the cw laser cavity will operate with constant pressure and gas velocity. (The constant velocity allows the following transformation: $x = vt$, where x, v, and t are the downstream position coordinate in the cw laser, the gas flow velocity, and time, respectively.) The only modification required to the program is to account for the change in gas density with temperature according to eq. (3).

The computer kinetics programs were used to establish the proper mixture ratio, fluorine dissociation percentage, and resonator coupling, and to predict laser performance. To keep the final combustion temperature $\lesssim 1000^{\circ}K$, we need to use large helium-to-fluorine

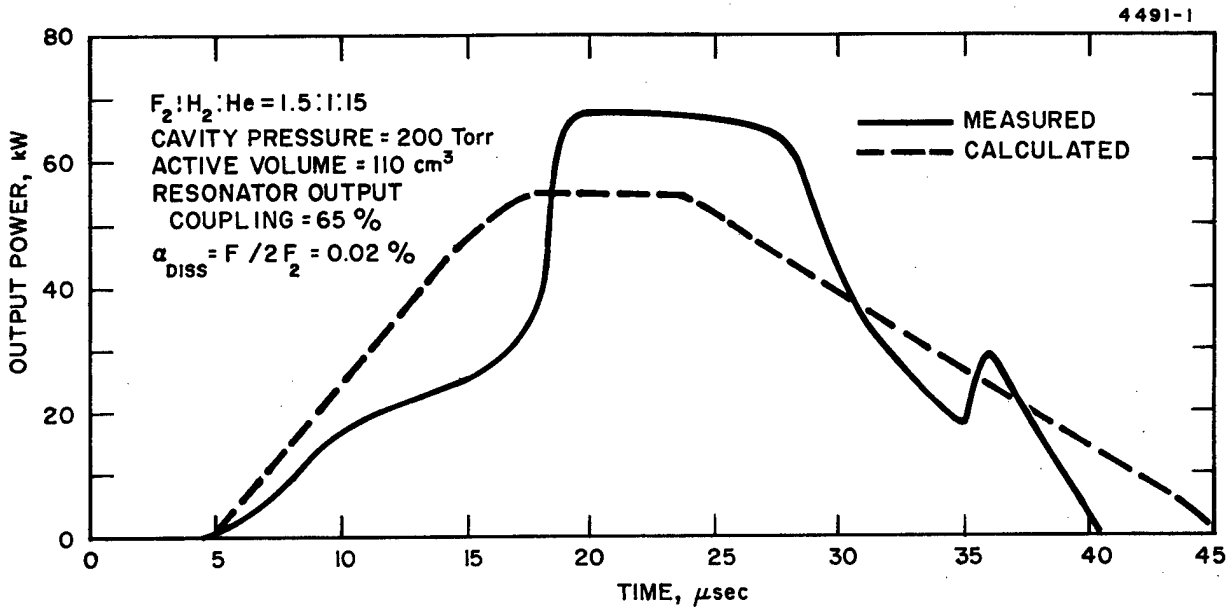

Fig. 1. Comparison of measured and calculated power for a flash-photolysis HF laser. Analysis assumed V^2 HF V-T dependence and $P(HF)\,\tau_{HF} = 0.0085$ μsec-atm.

ratios. We anticipate using a F_2:H_2:He mixture of 1:1/2:30 in the high-pressure devices. With this mixture ratio, and a flow Mach number M = 1.5, the predicted lasing lengths for various cavity pressures and initial fluorine dissociations are plotted in Fig. 2. For a cavity pressure of 200 Torr, the maximum lasing zone is approximately 6 cm with α_s = 0.2%. The lasing zone decreases for higher cavity pressures and at 800 Torr the lasing zone is only 2 cm for α_s = 0.2%. For cavity pressures of approximately 500 Torr, the expected lasing zone is 4 cm. The maximum value for the dissociation percentage α_s results from both e-beam limitations and heat input consideration in the discharge region and will be discussed more fully below.

In Fig. 3 the predicted specific power for a F_2:H_2:He mixture of 1:1/2:30 for various cavity pressures is given. Also given are the values for α_s which were used to maintain nearly constant specific power of 13 kJ/lb throughout the pressure range indicated. The fluorine dissociation varies from a maximum of 0.4% for a cavity pressure of 200 Torr or less to a low of approximately 0.1% for cavity pressures near one atmosphere. Since the product of the pressure and the fluorine dissociation is nearly constant, the electrical input power required to dissociate the fluorine should also remain constant. Assuming that 20 eV is required to dissociate a F_2 molecule,[4] the electrical efficiency for the results given in Fig. 3 is approximately 75%. By operating the device as a DF-CO_2 transfer laser, the specific power and electrical efficiency are predicted to increase to 50 kJ/lb and 350%, respectively.

3. Initiation

The selection of an initiation technique for the high-pressure cw device is governed by the following requirements:

- Well-localized initiation region
- Simultaneous initiation throughout the initiation region (no mixing)

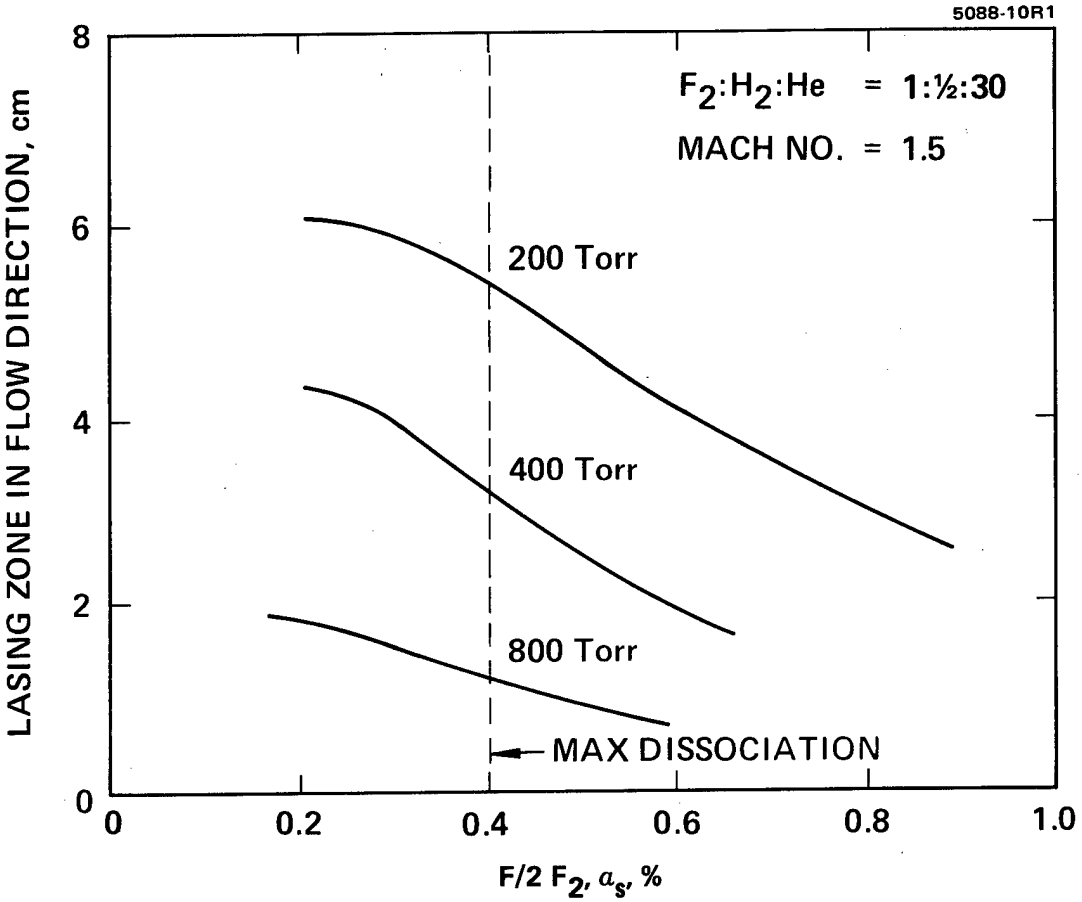

Fig. 2. Predicted lasing zone versus cavity pressure and fluorine dissociation, Mach number ≈1.5.

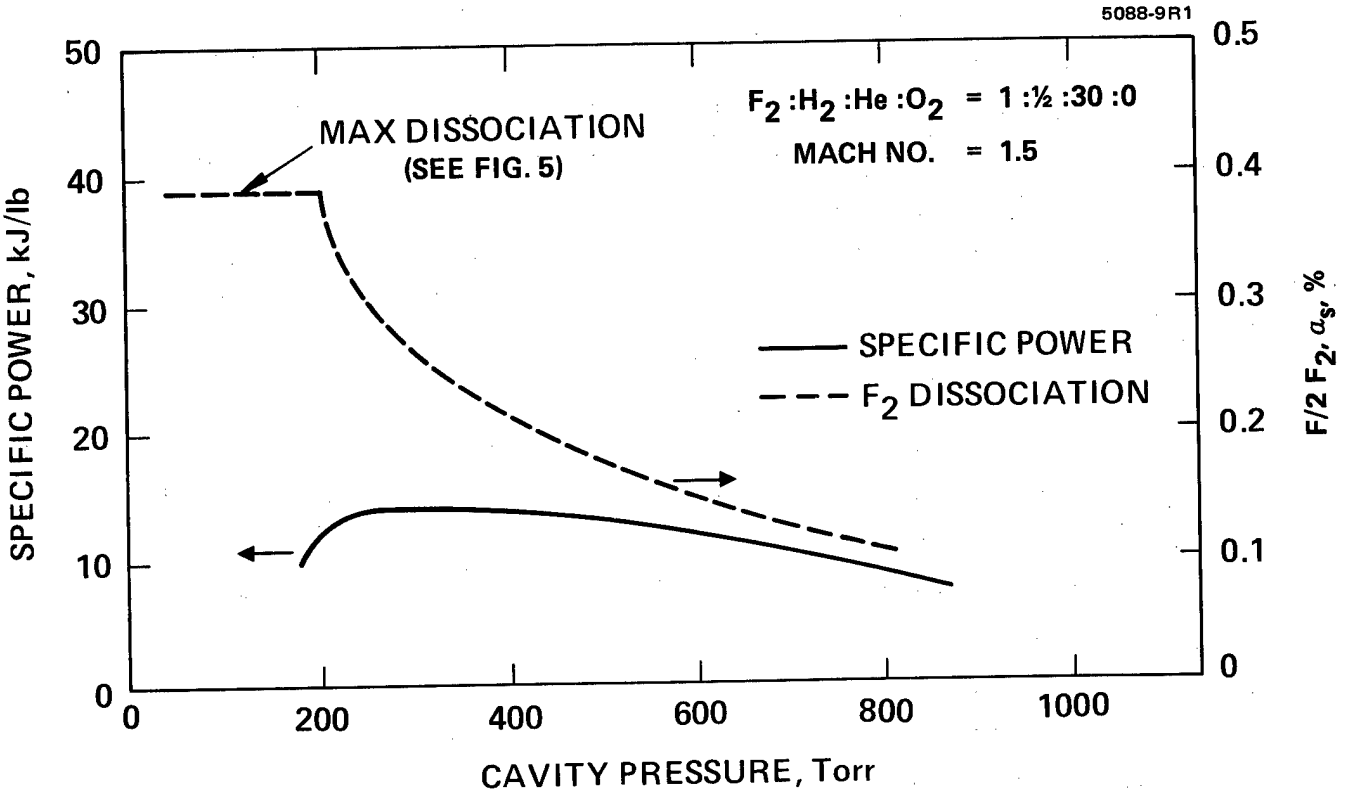

Fig. 3. Predicted laser performance versus cavity pressure, Mach number ≈1.5.

- Microscopic uniformity
- Efficiency

The only techniques that can satisfy the first three requirements are direct electrical discharge and ultraviolet photolysis. The final selection between these two alternatives is based on the high efficiencies which have been achieved with direct electrical initiation of pulsed H_2-F_2 lasers.

Achieving a stable, uniform glow discharge in a gas mixture containing fluorine is not a trivial task, particularly at high pressures. In the small-scale device, we pass a low-current-density electron beam (0.1 to 0.5 mA/cm^2) through the flowing laser medium to provide a uniform ionization. A dc voltage, also transverse to the flow, provides the energy input necessary for dissociating a small percentage of the F_2. Since it is necessary to operate the dc voltage at near breakdown conditions for efficient dissociation,[5] we use two different techniques to aid in stabilizing the discharge. First, we flow a stream of He and a small amount of SF_6 across each electrode. When the high-energy electrons pass through the streams, the gas is ionized and the resulting electrons will act as a "plasma electrode." The plasma will reduce the electric field near the electrode surfaces. The small amount of SF_6 prevents arcing downstream to the grounded dump tank. Second, the cathode electrode is a composition of polyester resin and carbon. The volume resistivity (adjusted by varying the amount of carbon) of the electrode is adjusted so that the total resistance is approximately 5 to 10% of the dc discharge resistance. For the small-scale device, the required electrode resistivity is approximately 10 to 20 kΩ-cm.

The volumetric input power required to dissociate a certain percentage of the molecular fluorine can be estimated from the following considerations. Referring to Fig. 4, the power deposited in the discharge region is given by

$$P_d = EJ_s LWH \tag{5}$$

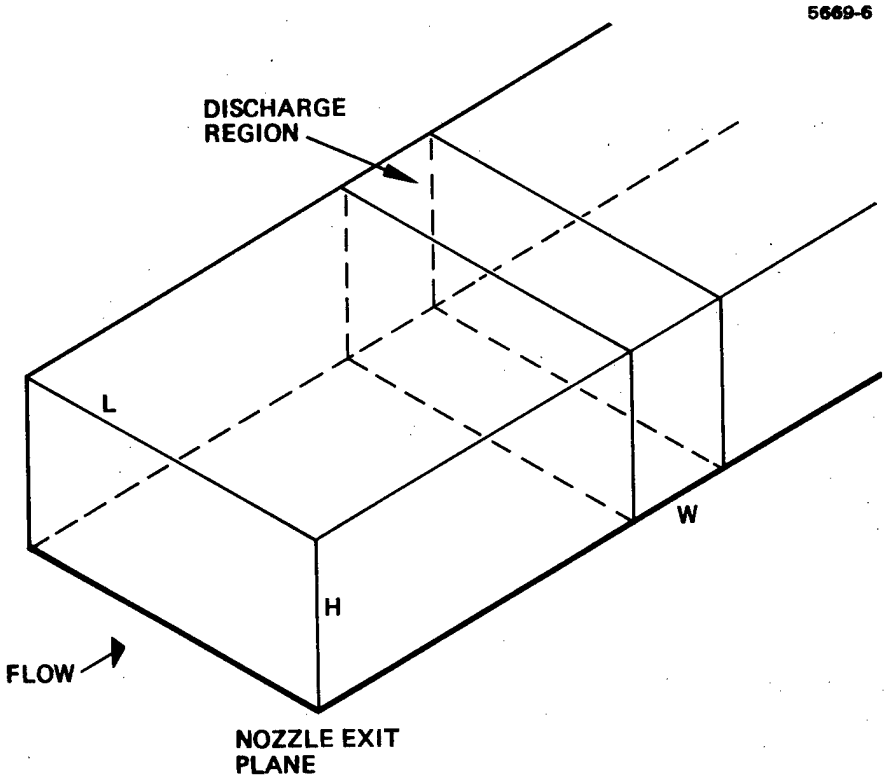

Fig. 4. Cavity configuration for transverse flow, chemical laser device.

where E is the electric field (V/cm) and J_s is the discharge current density (A/cm^2). The required energy to dissociate a F_2 molecule is given in Reference 4 as 20 eV/F_2 or 32×10^{-19} J/F_2. The amount of fluorine dissociated is simply given by

$$\alpha_s = F/2F_2 = \frac{EJ_sLWH}{F_2vLH\ 32 \times 10^{-19}} = \frac{EJ_sW}{F_2v\ 32 \times 10^{-19}} \qquad (6)$$

where v is the gas flow velocity and F_2 is the fluorine concentration. If we assume the total F_2 concentration is 0.3% and the electric field E is approximately the breakdown value of a mixture containing this amount of fluorine ($E \simeq 0.0175\ P(Torr)$, kV/cm), then eq. (6) can be rewritten as

$$\alpha_s = 17.5\ J_sWT(^oK)/v \qquad (7)$$

where T is the temperature of the laser gas.

From a simple analytical argument, we can show that the discharge current density J_s is only dependent upon the electron beam current density J_{eb} and not the cavity pressure for a constant discharge E/P. We can express J_s as

$$J_s = e\sum_i (\bar{v}_e N_e + \bar{v}_i N_i) \qquad (8)$$

where e is the charge of an electron, $\bar{v}_i$ is the average drift velocity of ion species i, and N_i is the concentration of species i. Both $\bar{v}_e$ and $\bar{v}_i$ are functions of E/P for a given gas mixture[6] and therefore are constant and independent of the cavity pressure if the discharge E/P is

maintained near the breakdown value. The steady state charge carrier density in an e-beam sustained discharge is given by

$$N = \left(Ne + \sum_i Ni\right) = Q_e/B \qquad (9)$$

where Q_e is the e-beam ionization rate and is proportional to the product of J_{eb} and pressure, and B is the overall loss rate due to attachment and recombination. Since both Q_e and B are proportional to pressure, J_s is independent of pressure when the discharge E/P is held constant. Further verification of this is given in Section IV where experimental results are discussed.

For a given flow velocity and discharge width W, the maximum fluorine dissociative, according to eq. (7), is limited by the maximum e-beam current density J_{eb}. For a non-cooled foil support the maximum cw current density is approximately 0.5 mA/cm^2. Experimental results on the demonstration device show that for $J_{eb} = 0.5$ mA/cm^2, the resulting $J_s \simeq 60$ mA/cm^2. Using this result for J_s, T = 175°K, and M = 1.5, eq. (7) reduces to

$$\alpha_s\Big|_{max} = W \times 0.0019 \qquad (10)$$

It should be pointed out here that eqs. (6) through (8) assume that $\bar{\nu}eNe \gg \bar{\nu}iNi$. In other words, it has been assumed that most of the discharge current is due to electron current. (In Section V we will show that this assumption is invalid and actually the discharge current is almost entirely ion current.)

Equation (10) is plotted in Fig. 5. According to eq. (10) the discharge width W could be increased indefinitely to reach a desired dissociation fraction, but in actuality the width is limited because of heat addition to the supersonic flow in the constant area discharge region. As heat is added by the chemical reaction and the discharge,

the flow Mach number decreases. When the Mach number reaches one, the flow chokes. The width at which this happens is also given in Fig. 5. The point where the two curves cross is the maximum dissociation fraction that can be obtained in a cw chemical laser with a flow Mach number M = 1.5. The maximum dissociation is approximately 0.4% and the required discharge width W = 2 cm. This discharge dimension was used in the demonstration device. According to Fig. 5, a cw e-beam sustained discharge should be capable of dissociating a sufficient amount of fluorine (see Fig. 3) for efficient operation if most of the discharge current consists of electron current.

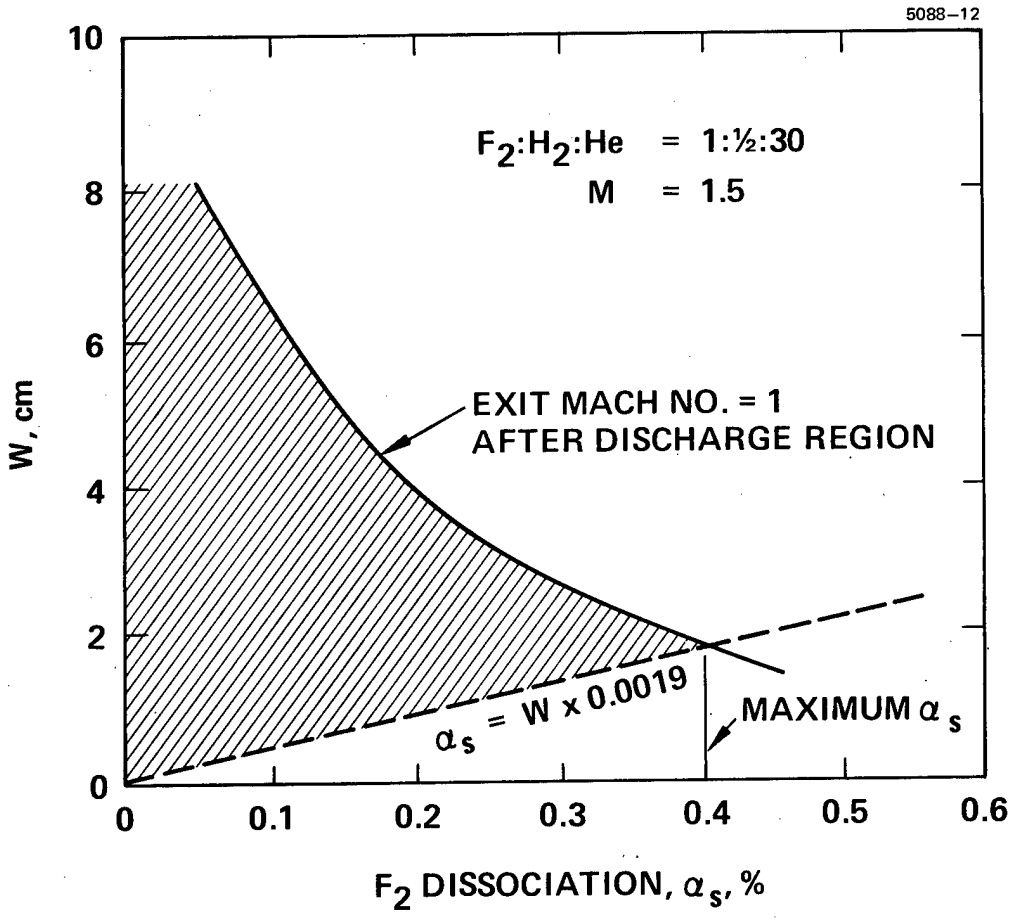

Fig. 5. Discharge width and fluorine dissociation limits.

III. DEMONSTRATION DEVICE DESIGN

This system is designed for cw chemical laser operation with a 15-cm^2 cavity cross section at pressures up to 500 Torr. A total gas mass-flow rate of 65 moles/sec at 1×10^5 cm/sec is available, with supersonic flow maintained for approximately 0.5 sec. A purge flow of 12 moles/sec of He/SF_6 for each discharge electrode is provided. The laser cavity is constructed using smooth walls to prevent medium disturbances. The electrical discharge system is designed to provide conditioning of the gas between the discharge electrodes using a plasma cathode e-gun, and provides uniform field enhancement via an energy storage capacitor bank. The top and bottom cavity walls have a variable divergence angle to maintain constant pressure during the chemical reaction in the downstream direction.

A. Mechanical

Major components of the gas-handling and laser apparatus are shown schematically in Fig. 6. The main flow duct has a cross section of 2.5 cm x 6 cm with the laser axis and discharge electrodes situated transverse to the flow direction. Reactive gases are diluted with helium and stored in two 3 ft^3 tanks. The top and bottom cavity walls are purged with a mixture of He and SF_6 which is premixed and stored in a 5.5 ft^3 tank. Gas flow is initiated by activation of fast acting pneumatic valves attached to each storage reservoir. Cavity pressure is controlled by orifices in the exhaust lines of the tanks. The fuel and oxidized gases are combined by means of an injector which produces alternate parallel flow streams of 0.75 mm thickness. The streams mix together by turbulence and diffusion in a slightly converging duct approximately 50 cm long. The three one-dimensional supersonic nozzles, one each for the electrode purge flow and one for the laser gas mixture, are located at the entrance to the laser cavity. The discharge electrodes are located approximately 5 cm downstream

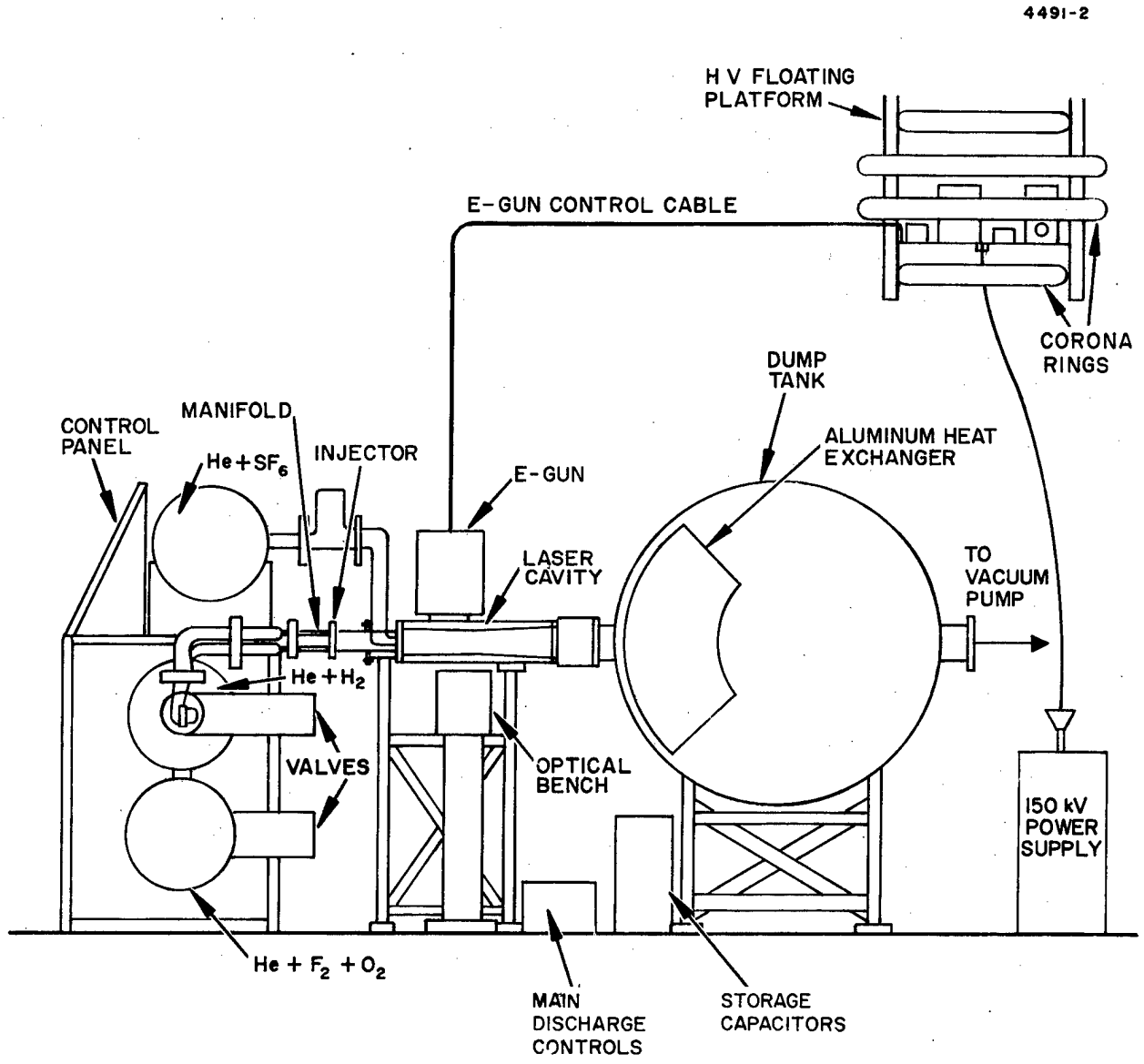

Fig. 6. Side view of HF/DF cw chemical laser system.

from the nozzles. The entire laser cavity is constructed of Plexiglas for electrical insulation. The downstream portion of the cavity contains Teflon inserts which form the top and bottom walls. These inserts allow the wall divergence angle to be varied.

Before the flow enters the dump tank, nitric oxide is injected into the flow stream with a stainless steel spray bar; this allows the unused gases to react gradually while passing through the heat exchanger in the 90 ft^3 dump tank. The heat exchanger consists of an array of 0.030 in. thick aluminum plates spaced 0.200 in. apart across the entire 44 in. duct width. A blower-vacuum pump combination operating at 300 CFM exhausts the gases to a final system pressure of 1.6×10^{-5} atm between runs. A photograph illustrating major features of the apparatus is given in Fig. 7.

Details of the injector design are shown in Fig. 8. As depicted in Fig. 9, the individual stainless steel plates are assembled in 10 cm segments. The plates were prepared for brazing by coating with nickel followed by copper. Each segment was assembled and brazed at 1100°C for approximately 1 hour using a gold-based brazing material (Nicoro No. 80). A photograph of a section of the final assembled injector array is shown in Fig. 10.

1. Nozzles

The purpose of the three supersonic nozzles is to accelerate the flow to M = 1.5 while maintaining parallel flow at the nozzle exit. The center nozzle shown in Fig. 11 accelerates the premixed gases F_2 + He + O_2 to M = 1.5 using an area ratio $A/A^* = 1.16$. The expansion contour of the nozzle was designed using the method of characteristics; it was assumed that the gas flow entering the nozzle was uniform and parallel.[1] The expansion rate of the nozzle was purposely made to be slow to prevent flow separation. The distance between the throat and exit is approximately 2 cm, and the nozzle exit height is 1.5 cm. The boundary layer thickness for our flow conditions is estimated at 0.5% of the throat height.

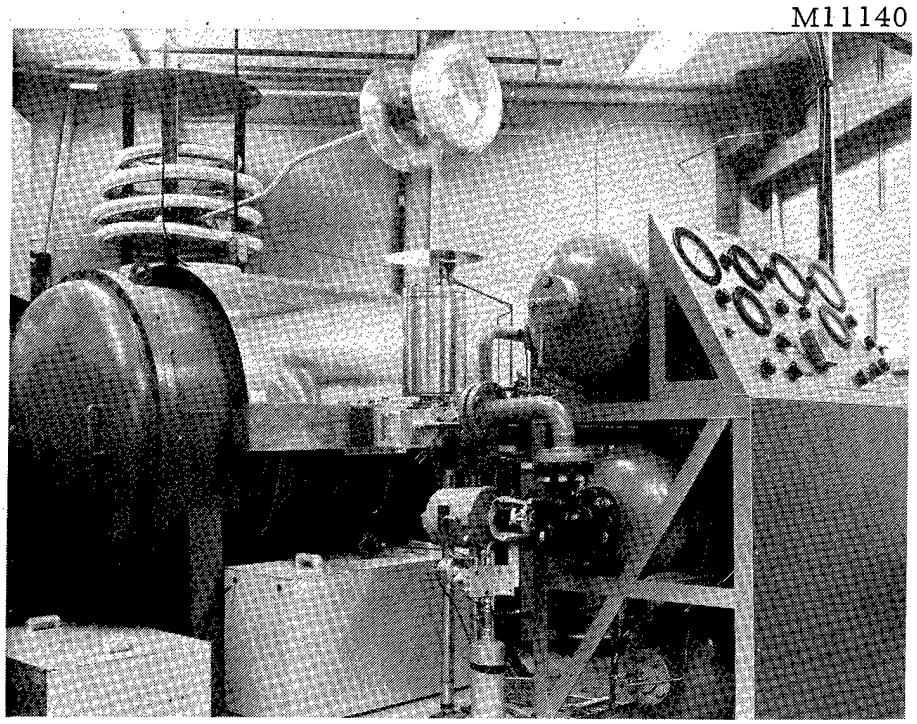

Fig. 7. Photograph of cw HF/DF chemical laser system.

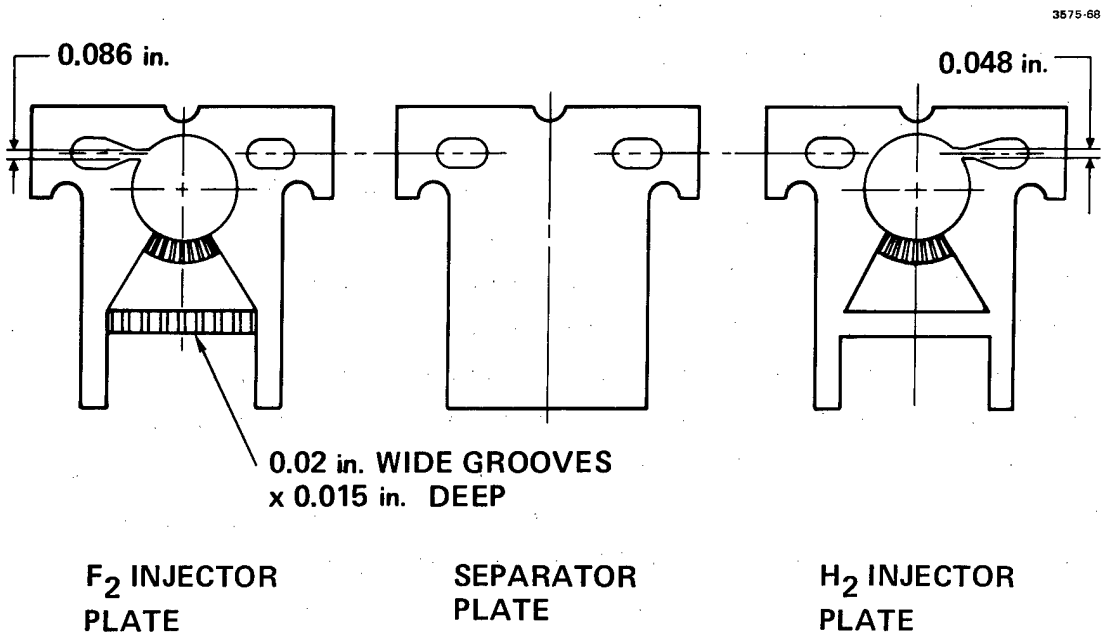

Fig. 8. Design of individual injector plates.

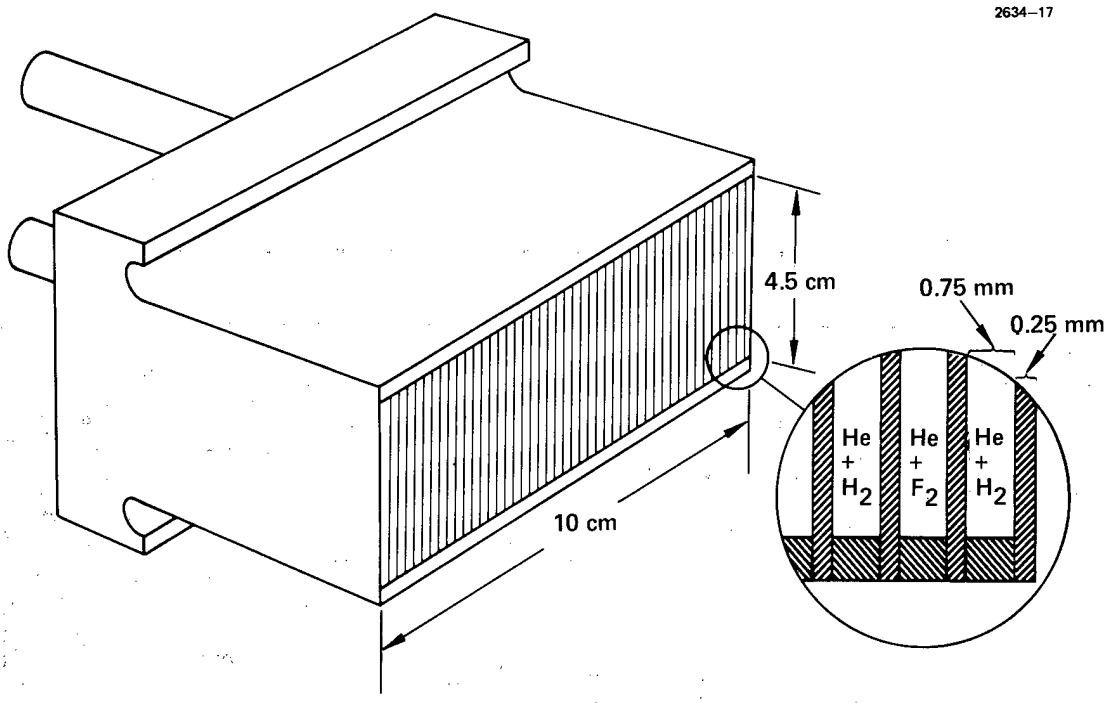

Fig. 9. Assembled segment of injector system.

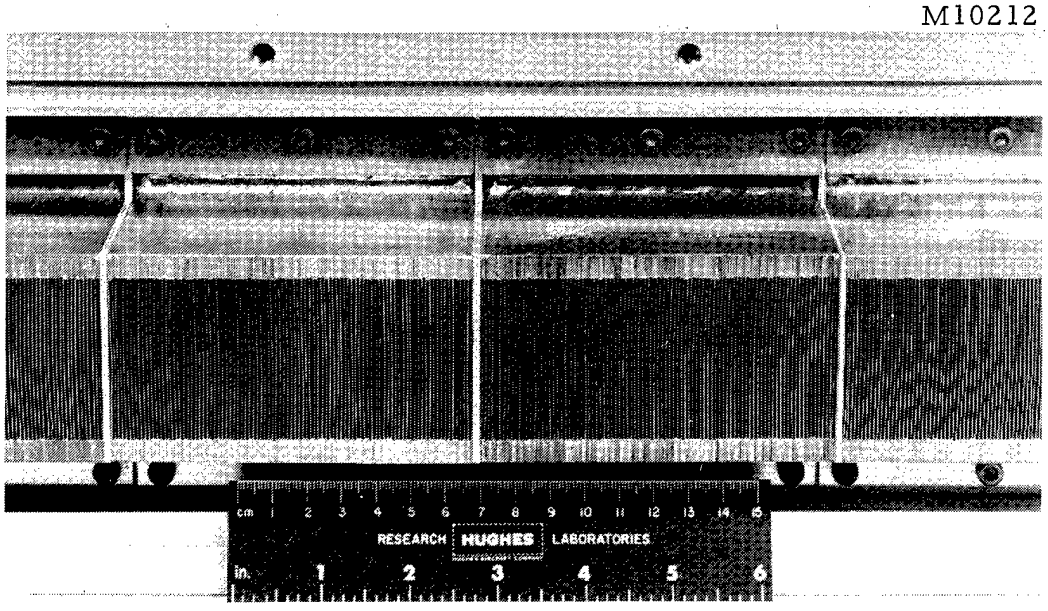

Fig. 10. Photograph of injector system after final stage of fabrication.

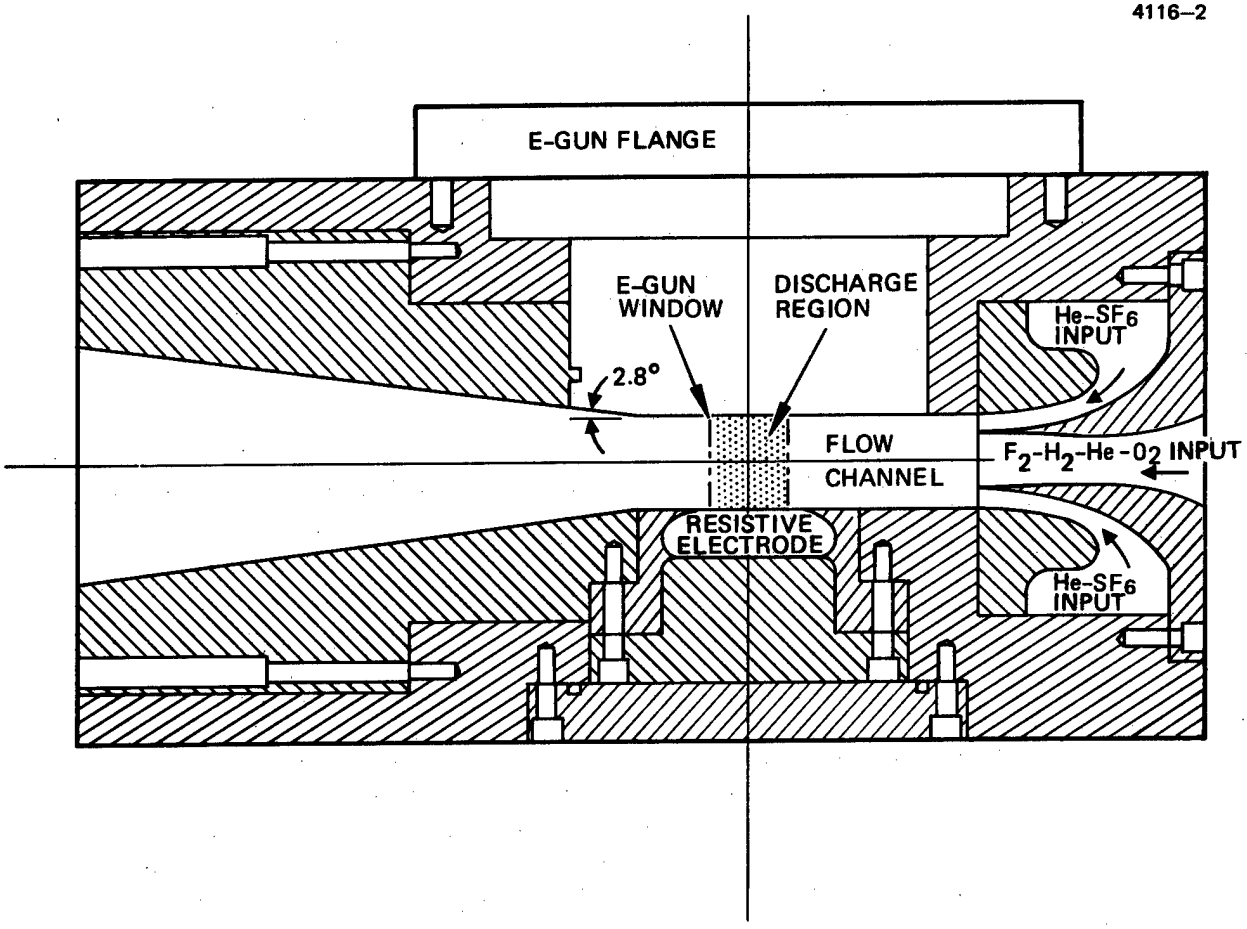

Fig. 11. Cross section of flow channel for small-scale demonstration device.

To provide a parallel stream of He-SF_6 above and below the laser gas stream with a minimum of separation between the two streams at the nozzle exit plane, it was necessary to use a Prandtl-Meyer[1] turn to accelerate the He-SF_6 stream to M = 1.5. The nozzle turns through an angle of approximately 11^o over a distance of 2 cm between the nozzle throat and exit plane. The nozzle throat and exit height is 0.5 cm. A photograph of the assembled nozzle is shown in Fig. 12. The gas flow for the top and bottom nozzles enters from both sides of the nozzle assembly while the gas flow for the center nozzle enters from the back side.

2. Laser Flow Channel

The laser flow channel houses the nozzle assembly, resistive electrode, side viewing windows, diagnostic probes, and Teflon inserts, and supports the plasma cathode electron gun. The housing was fabricated from a single piece of Plexiglas. The side windows, which are also Plexiglas, act as the walls for the 6-cm wide flow channel. Both sides of the windows are polished to permit viewing the flow channel. One of the windows, as shown in Fig. 13, contains 10 probe holes to permit pressure transducers or thermocouples to be inserted into the flow. When a probe location is not in use, it is plugged with a Teflon insert.

B. Electrical

The main electrical discharge system consists of a resistive anode and a flat 0.0005 in. aluminum foil cathode through which high energy electrons pass for preionization of the gas mixture. The anode is a composition of polyester casting resin and carbon. The volume resistivity provides a stabilization mechanism against the formation of arcs within the plasma.[7] Since large fluorine dissociation efficiencies (~10%) require the plasma ϵ/N to be near breakdown values, stabilization techniques are necessary to achieve cw electrical discharges in fluorine gas mixtures. The resistive electrode provides a means for

M11047

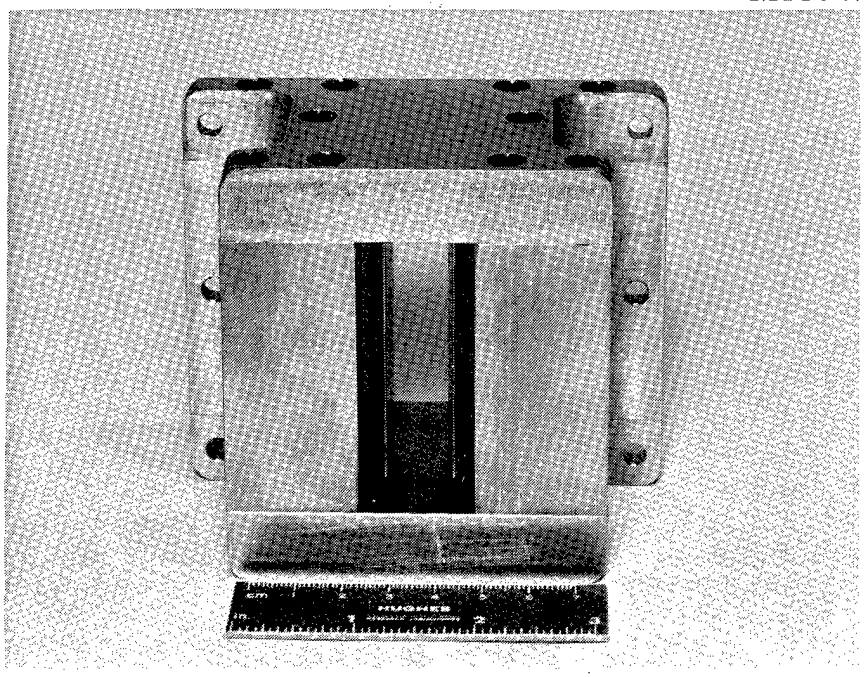

Fig. 12. Photograph of nozzle assembly.

M11046

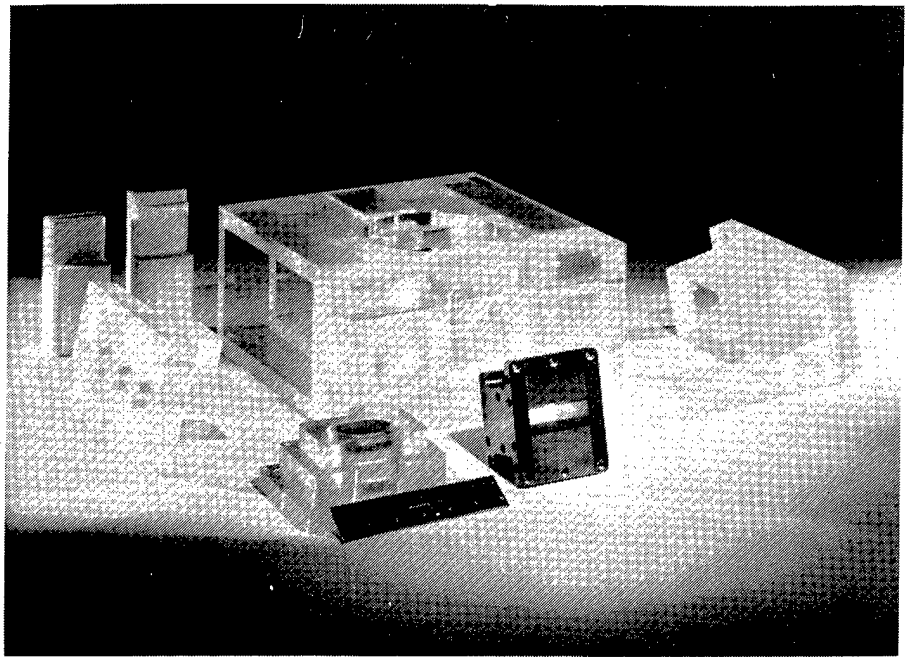

Fig. 13. Photograph of disassembled laser flow channel.

ballasting an arbitrarily large number of "electrodes" each carrying a small current.

A volume resistivity of 10 to 20 kΩ-cm (total resistances of ~1.5 kΩ) was selected for the electrode. This corresponds to approximately 10% of the plasma resistance for a F_2:H_2:He = 1:1:30 and a discharge E/P near breakdown valves. The electrode was machined from a rectangular-shaped polyester mold containing approximately 15% carbon by volume. The electrode profile is a plano-elliptic contour which is flat over a region ~1.3 times the discharge width and then joins smoothly to an ellipse with a ratio of major-to-minor axis of 1.5 to 1. The flat portion of the electrode is 2 cm x 4 cm. The flat portion of the electrode was not extended to 6 cm to prevent arcing at the side walls. The electrode mounted in a Plexiglas holder is shown in Fig. 13.

The main discharge power supply circuit is shown in Fig. 14. A capacitor storage bank of 14 to 26 μF is used to supply a nearly constant voltage to the electrodes for ~100 msec. Because the amount of charge required to dissociate a given amount of F_2 is independent of pressure, but the required capacitor voltage (or stored charge) decreases with pressure, more capacitance is required at low cavity pressures to maintain a nearly constant discharge voltage during a run. The high voltage (HV) vacuum relay (TURN ON) holds off the discharge voltage until the cavity pressure reaches a prescribed value. This prevents large E/P's and arcing during startup. The "crowbar" vacuum relay places a 7 kΩ resistor across the capacitor bank at approximately 60 to 100 msec after the discharge voltage is applied to the electrodes. This prevents late time arcs from occurring since the cavity pressure falls exponentially in this type of "blowdown" system, causing the E/P to reach breakdown values if the voltage is not removed.

1. Electron-Gun

A schematic diagram of the plasma cathode electron gun is shown in Fig. 15. The device consists of three major regions: (1) the plasma generation region in which the beam electrons originate,

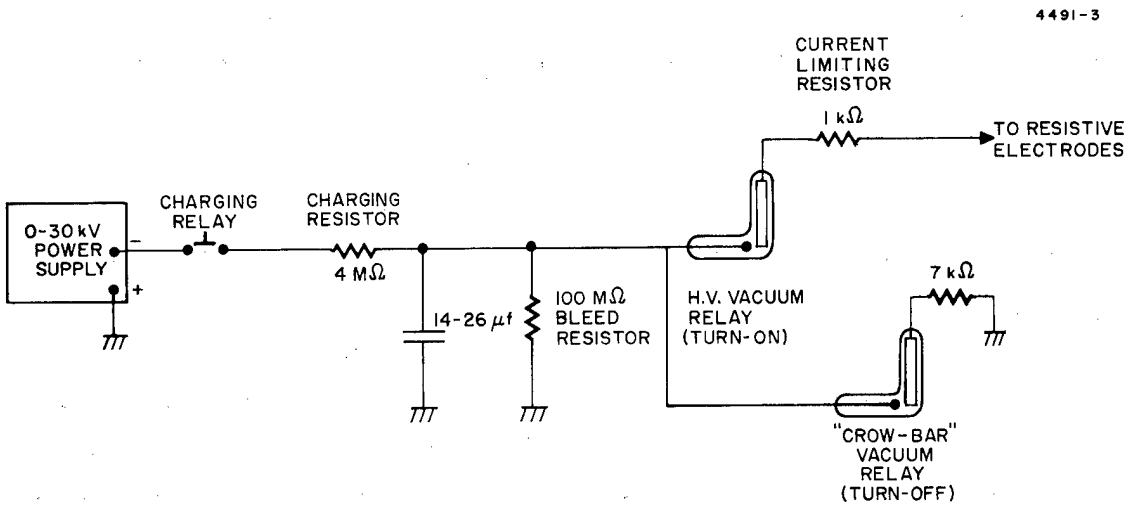

Fig. 14. Schematic diagram of main discharge power supply circuit.

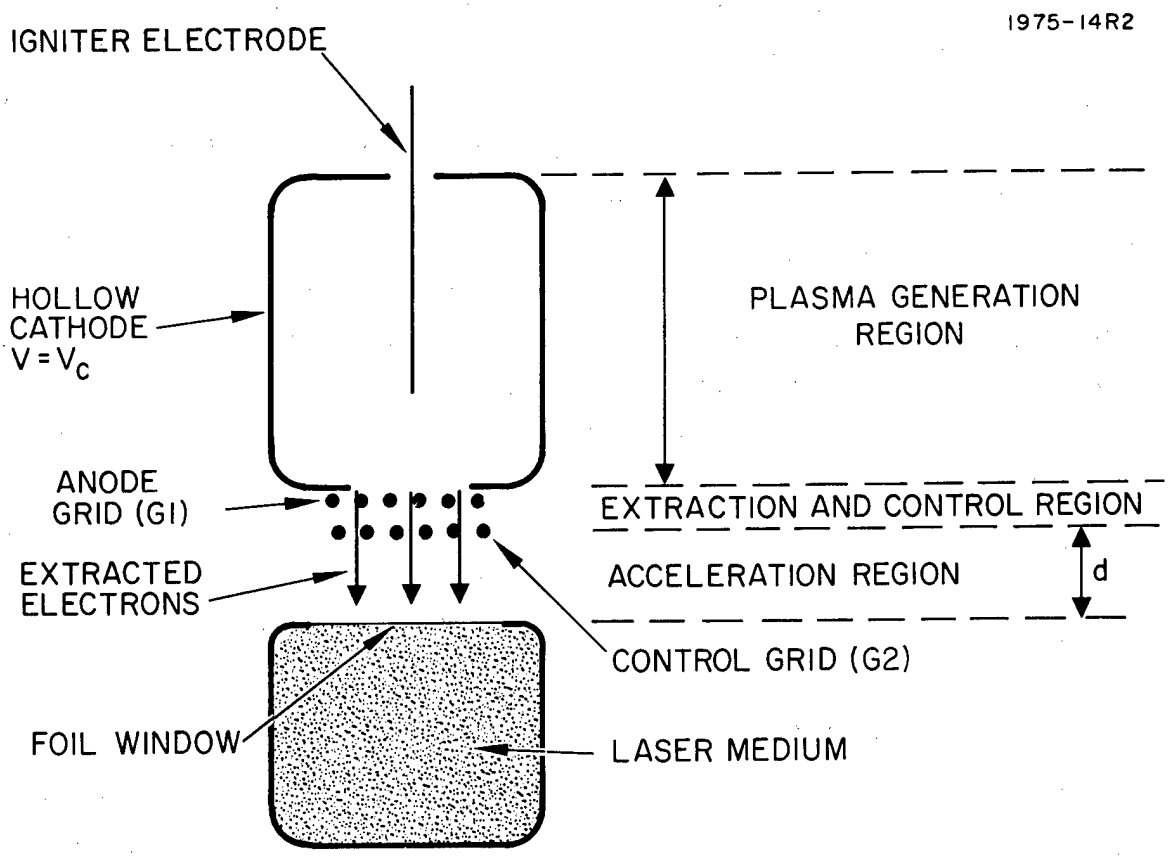

Fig. 15. Schematic of the plasma cathode electron gun.

(2) the extraction and control region where electrons are extracted from the plasma and transported in a controlled manner into the acceleration region, and (3) the high-voltage acceleration region where the electrons are accelerated to high energies prior to passing through a thin metal foil window and into the laser medium. These regions are comparable to the thermionic cathode, control grid, and grid-to-anode space of a conventional triode.

The plasma generation region in the present device consists of a low-pressure glow discharge struck between the cold, hollow cathode surfaces and the anode grid, G1. This type of discharge has been chosen because of its stability, reliability, simplicity, and ability to operate at the low gas pressures required to preclude gas breakdown in the acceleration region. In the present application, the discharge operates at a voltage, which is approximately independent of current, of typically 400 to 700 V with helium at pressures typically in the range of 10 to 50 mTorr. Helium is used because He^+ ions have relatively low sputtering yields and because helium has high-voltage breakdown characteristics which are superior to those of other gases.

The major characteristic of the hollow cathode discharge is that most of the plasma volume is surrounded by the cathode surface. The discharge, which is sustained by secondary electron emission due to ion bombardment of the cathode surface, is operated in a region where the rate of ion generation by ionization in the discharge volume is sufficient to maintain the plasma potential slightly above anode potential. Electrons are extracted from the discharge plasma through the anode grid, G1, and pass through the control grid, G2, into the acceleration region. Voltages of typically 0 to -100 V relative to G1 are applied to G2 to control the beam intensity from maximum to near cutoff. Grid G2 also serves to provide isolation between the low-voltage discharge region and the high-voltage acceleration region. Alternatively, control of the beam current is possible through variation of the hollow cathode discharge current through the potential of G1.

A photograph of the e-gun with the hollow cathode removed is shown in Fig. 16. Visible at the end of the cathode is the control grid, G2. The window holder is in the lower portion of the photograph. The foil window is mounted on an aluminum-ribbed structure to aid heat conduction away from the foil during operation. The window transmission area is 2 cm x 4 cm, and the window exit plane is flush with the window holder. A photograph of the e-gun assembled and mounted on its test stand atop the diffusion pump station is shown in Fig. 17.

A schematic of the e-gun control circuit is shown in Fig. 18. All components, excluding the power supply and e-gun, are mounted on an electrically floating platform, shown in Fig. 19. Two dc-dc converters, powered by two series connected 12 V batteries, are used to drive the e-gun ignitor and anode grid G1. The use of the dc converters eliminates the need for bulky isolation transformers. Voltage to grid G1 is controlled by a switching relay which in turn is controlled by signals received by means of an optical fiber. An RC network on the output of the anode power supply increases the rise time of the turn-on signal to 2 msec. The wires connecting the e-gun with the floating platform are enclosed in 1 in. conduit, and connections are made between the two toroids shown in Fig. 19.

Proper sequencing of the e-gun and main discharge as well as sequencing of the gas control valves is essential for operation of this device. The electrical system which performs this function is shown schematically in Fig. 20. The electrical discharge sequence is delayed approximately 450 msec to allow the gas valves to open and the pressure in the cavity to reach its operating value. Once the proper cavity pressure is reached, the e-gun is turned-on; this is followed 10 msec later by the main discharge voltage. The shutdown sequence begins approximately 50 to 60 msec later with e-gun turn-off followed 15 msec later by the main discharge.

M10890

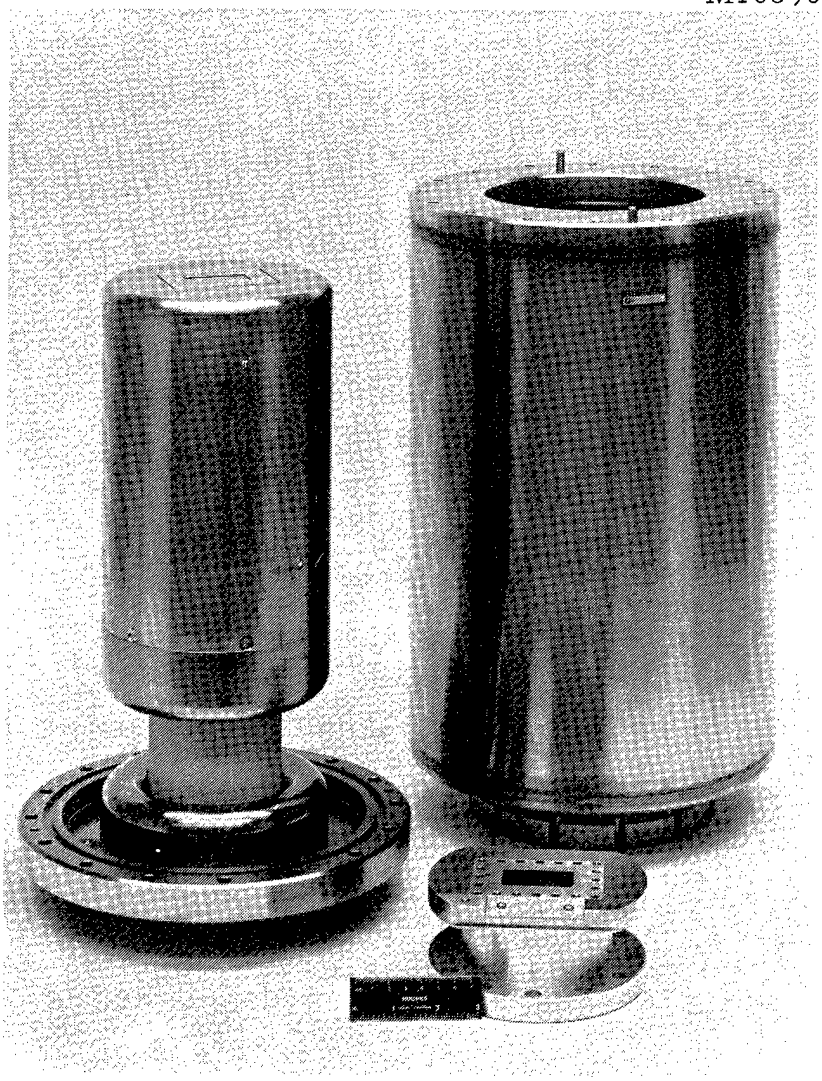

Fig. 16. Disassembled plasma-cathode electron gun showing hollow cathode.

M11008

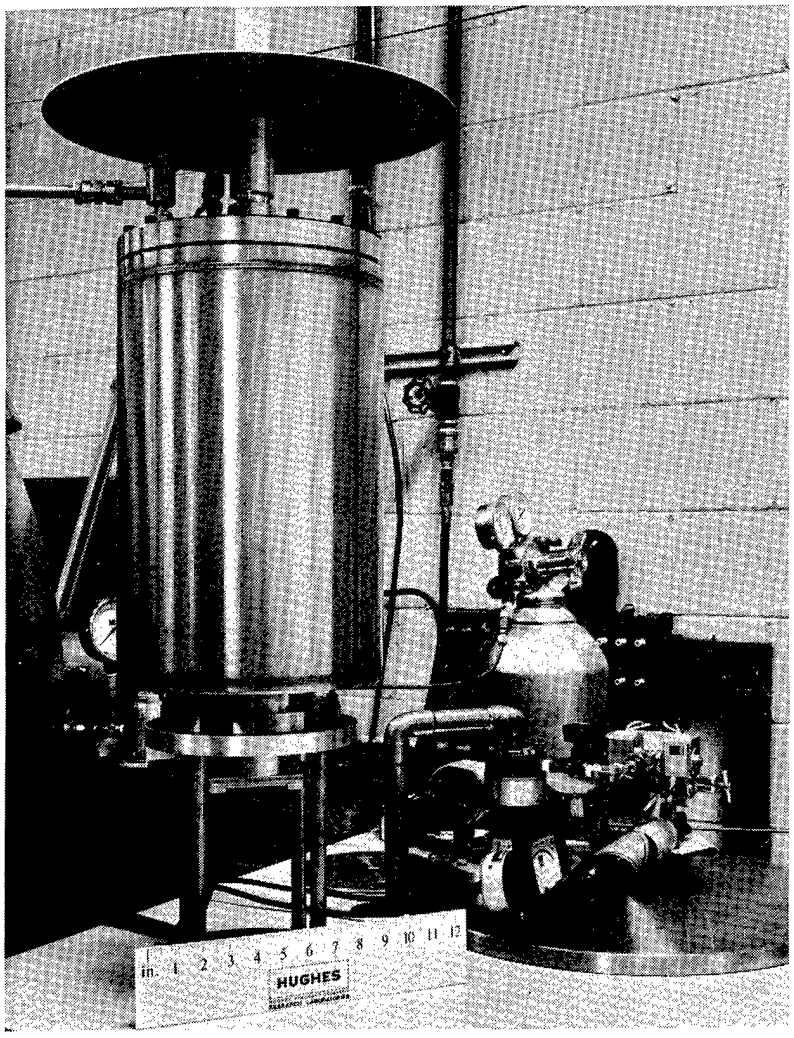

Fig. 17. Electron gun mounted in test stand.

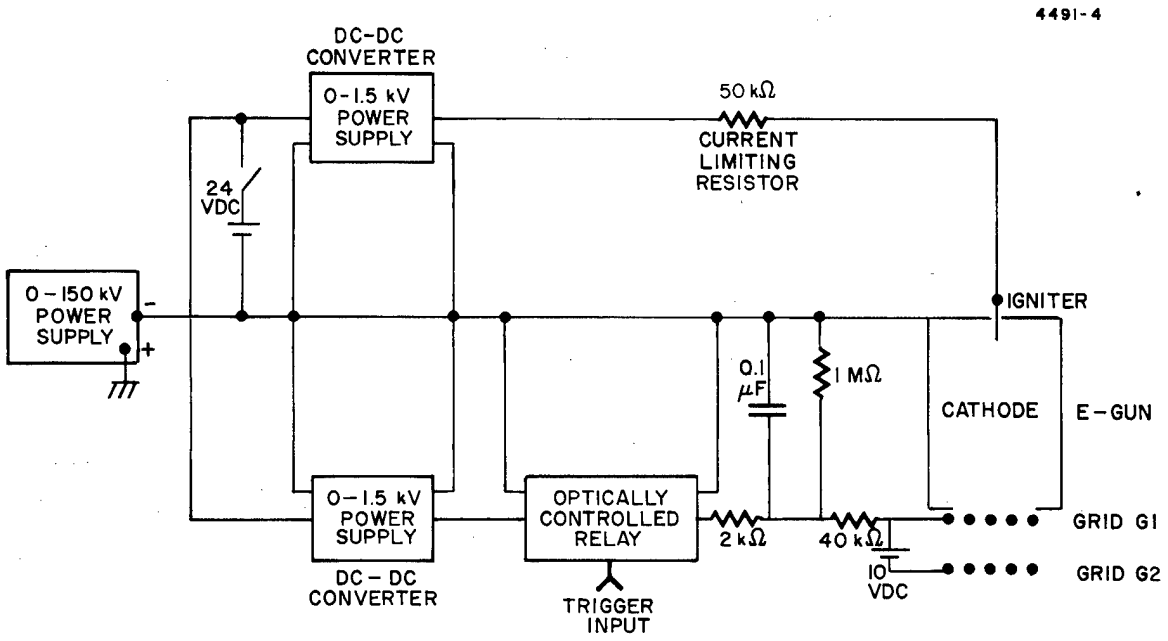

Fig. 18. Schematic diagram of electron gun control circuit.

M11007

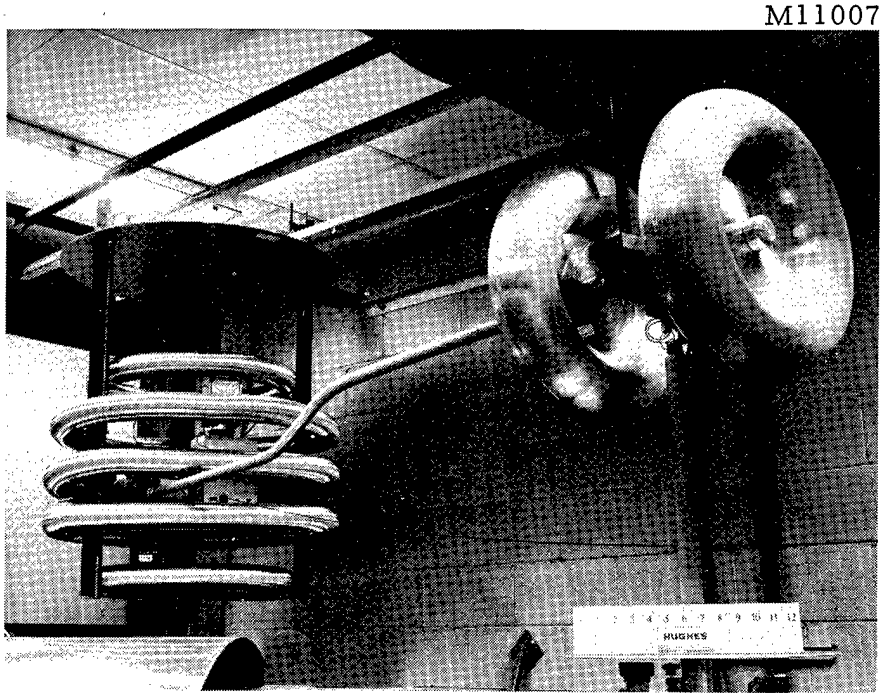

Fig. 19. Photograph of high voltage platform for electron gun control circuits.

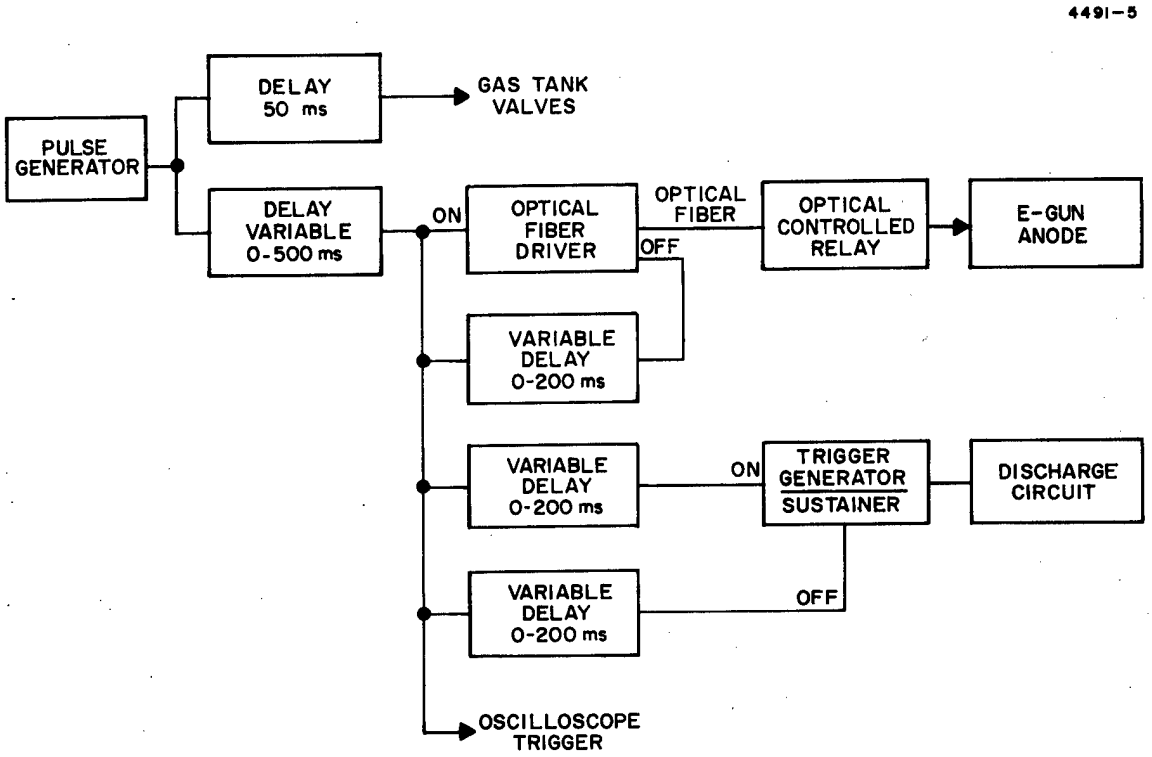

Fig. 20. Schematic diagram of electrical control system for cw HF/DF chemical laser.

C. Gas Flow Calibration

The mass flow rate and pressure in the laser cavity depend upon the open areas of the injector system and orifice plates, the stagnation pressure in the storage tank, and the opening characteristics of the control valves. Flow tests were conducted to establish quantitative relationships between these parameters.

Total molar flow rates were measured by pressure transducers in the storage tanks. Because the gas mixture ratio F_2:H_2:He = 1:1:30 is fairly dilute, the tests were made with pure helium. The values obtained for the 3 ft^3 and 5.5 ft^3 storage tanks are shown in Fig. 21. Orifice sizes for the feed lines from the 3 ft^3 and 5.5 ft^3 tanks were derived from the following equation

$$F = \rho V A \text{ moles/sec} \qquad (11)$$

where ρ is the gas density in the cavity, V is the gas velocity, and A is the nozzle exit area. The laser nozzle area A_L is 9 cm^2, and the area for the two electrode surge nozzles is 6 cm^2. The gas velocity V for M = 1.5 is 1×10^5 cm/sec. Once a pair of orifice sizes was selected, cavity pressure was verified by a pressure transducer in the cavity side wall. A typical time response of the storage tank and cavity pressure for a peak cavity pressure of 200 Torr is shown in Fig. 22.

To prevent chemical instability, small amounts of oxygen were added to the F_2-He storage tank, and the valve on the H_2-He tank was opened approximately 30 msec before the F_2-He-O_2 valve.

Characteristics of the device are given in Table 1.

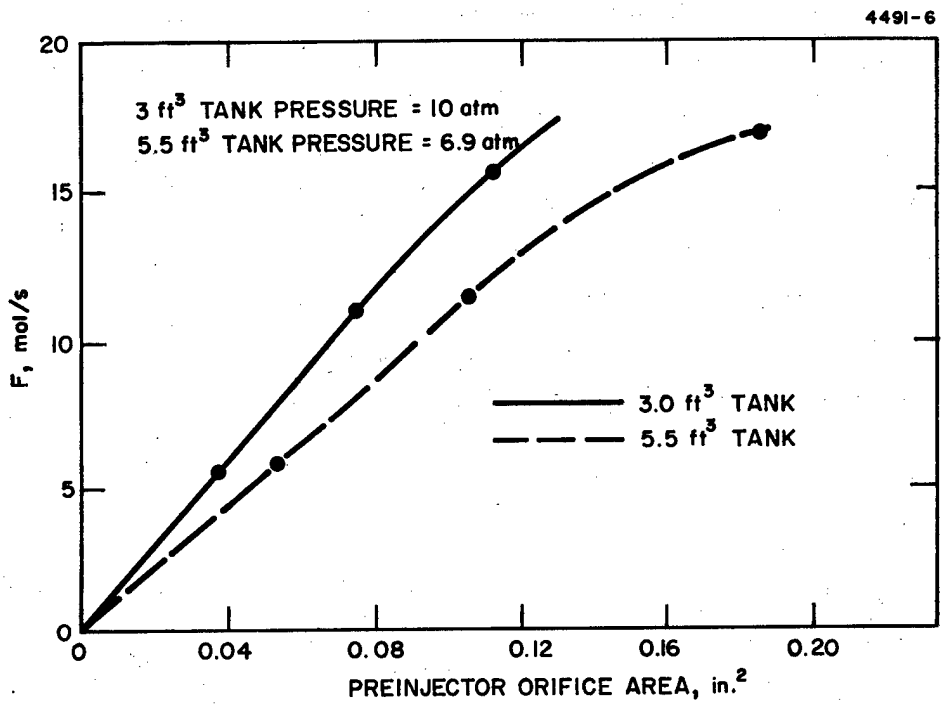

Fig. 21. Gas flow calibration for 3 ft^3 storage tanks; molar flow rate versus preinjector orifice size.

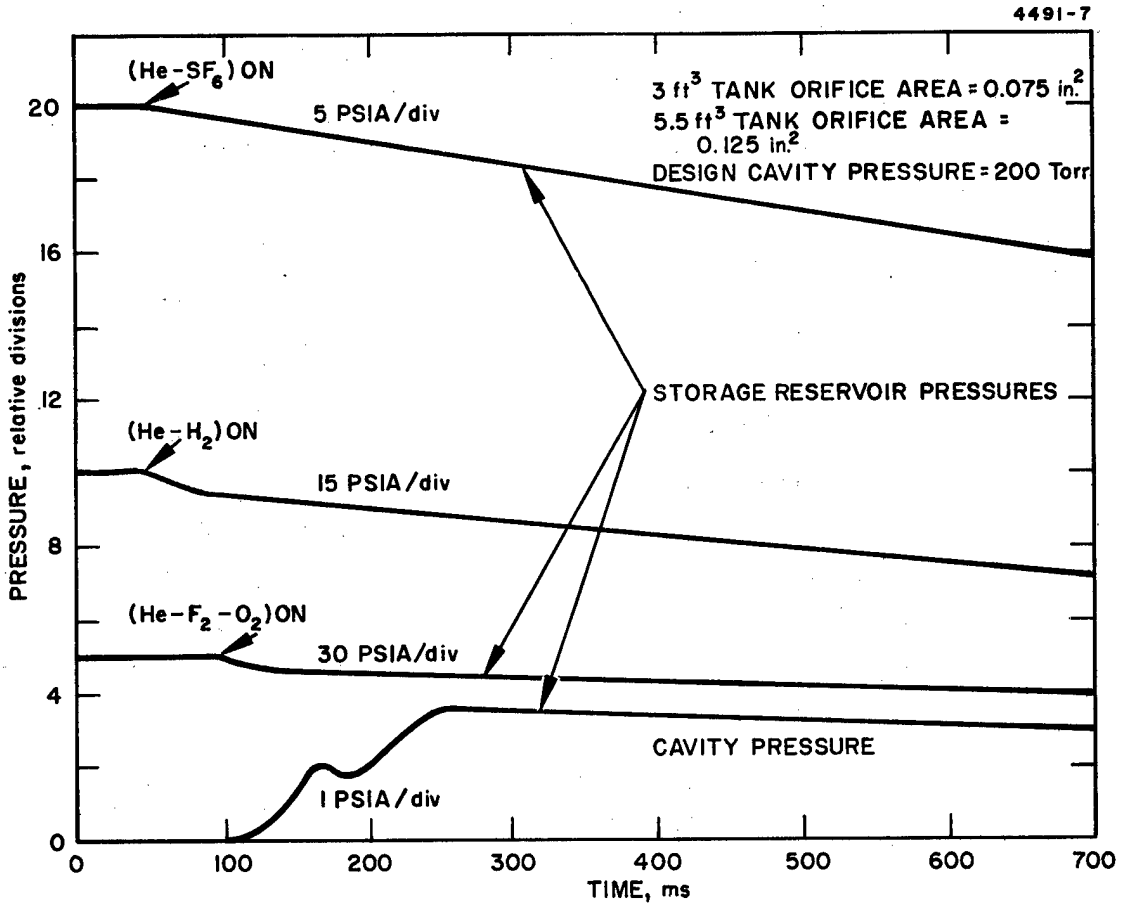

Fig. 22. Oscillograph traces showing pressure responses of the cw HF/DF chemical laser system.

TABLE 1. Device Description

Nozzle Area	
Electrode purge flow	6 cm^2
Laser flow	9 cm^2
Flow Capabilities	
Electrode purge flow	125 g/sec
Laser flow	190 g/sec
Fluorine mass flow	≤12 g/sec
Flow velocity	1000 cm/sec
Laser duct pressure	≤500 Torr
Electrical	
E-beam (140 kV) preionization	0 to 0.5 mA/cm^2
Main discharge:	
Voltage	0 to 25 kV
Capacitor storage bank	14 to 26 μF
Discharge on time	~100 msec

IV. EXPERIMENTAL RESULTS

A. Supersonic Flow

Data on electrical discharge measurements consists of oscilloscope traces of sustainer voltage and current and of e-gun cathode current, and time-integrated photographs of the discharge region in the flow channel. In order that the reader might interpret the traces, the important dimensions of the flow channel are given in Fig. 23 and a photograph of the flow channel taken through the polished Plexiglas side window is shown in Fig. 24. The photograph clearly shows the electron gun window, the 10 diagnostic probe holes located in the opposite side window, and the diverging top and bottom channel walls. Not visible in the photograph is the resistive electrode located directly below the e-gun window.

An initial experiment was performed to determine if the three supersonic streams maintained parallel flow or if they mixed together by turbulence caused by a difference in nozzle exit conditions. A time-integrated photograph of the radiation from the e-beam firing into the cavity at 100 Torr of pure helium was compared with a photograph taken under identical conditions except the electrode purge flows contained 3% Ar and the laser stream flow contained 3% F_2. The two photographs are shown in Fig. 25. The photograph taken with F_2 in the flow shows less illumination coming from the center flow stream than from the two electrode flow streams. Although the contrast in the photographs is poor, the results clearly show that flow separation is being maintained.

Electron-beam sustained discharge measurements were made at cavity pressures of 100, 200, 300, and 400 Torr. Initial runs with pure helium in the electrode stream flows were unsuccessful because of the main discharge voltage causing breakdown in the helium to upstream and downstream device grounds. To eliminate this problem we added approximately 2-3% SF_6 to the helium flow.

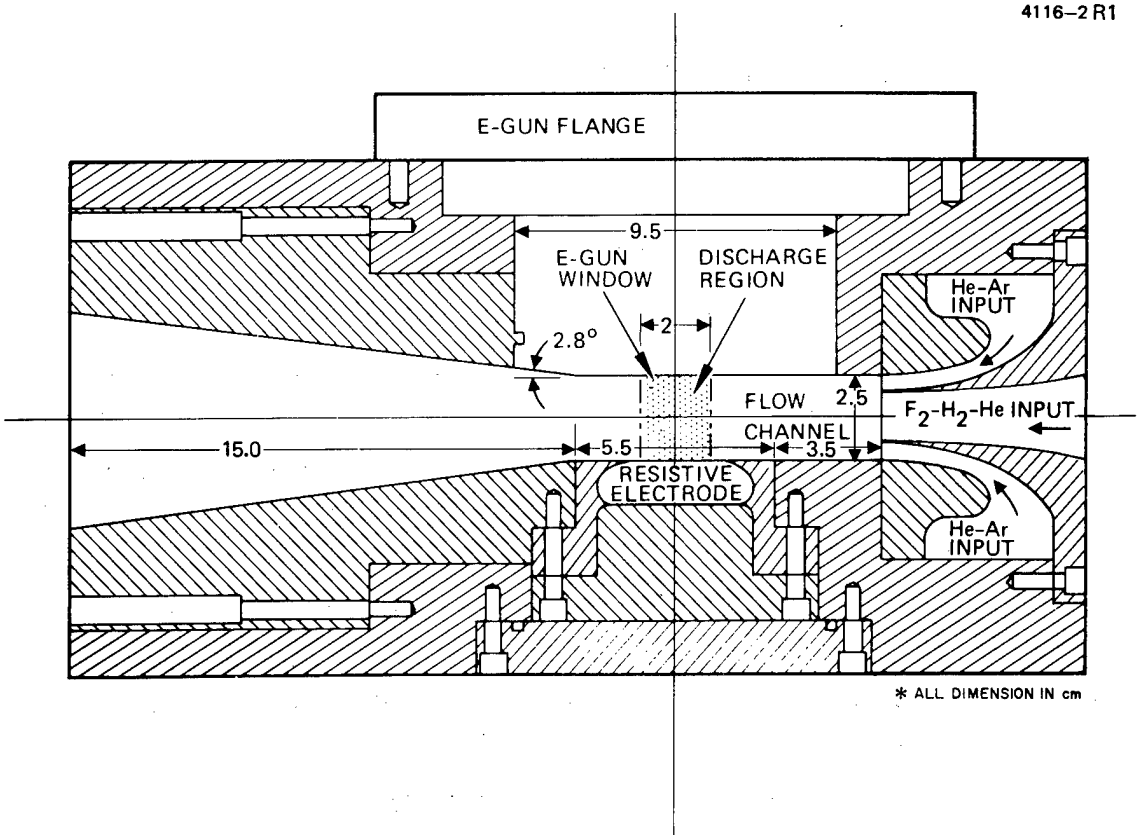

Fig. 23. Cross section of flow channel for small-scale demonstration device.

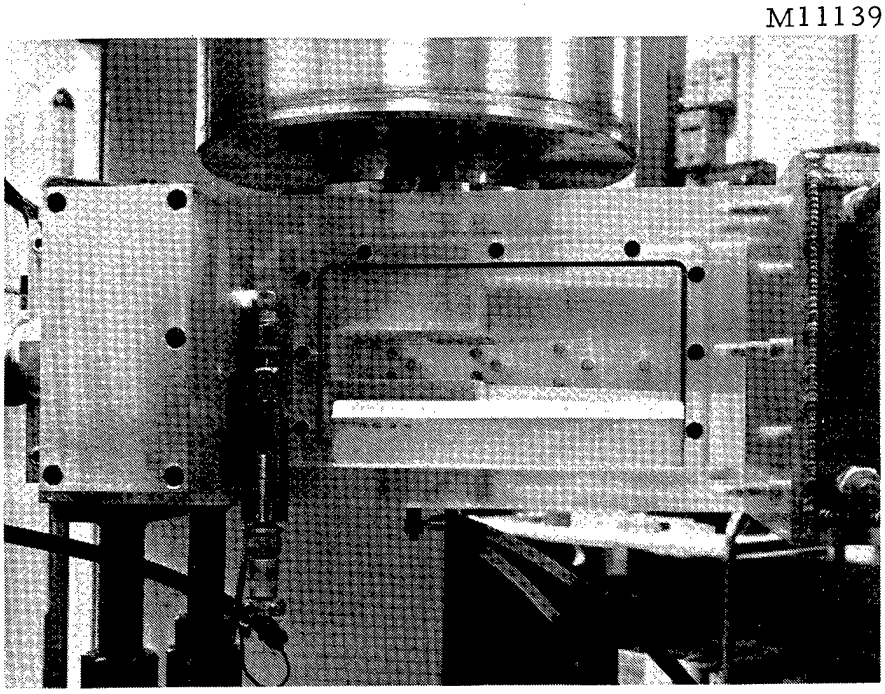

Fig. 24. Photograph of flow channel.

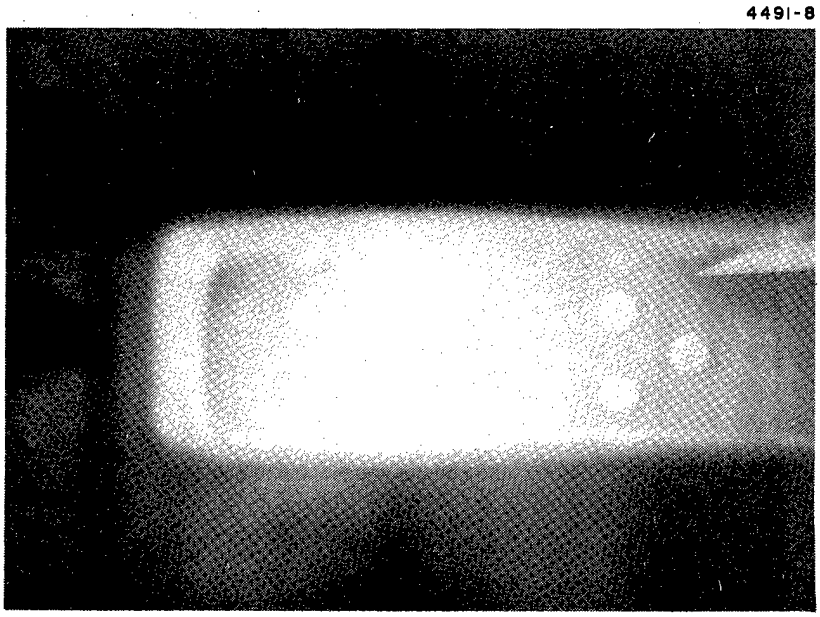

(a)

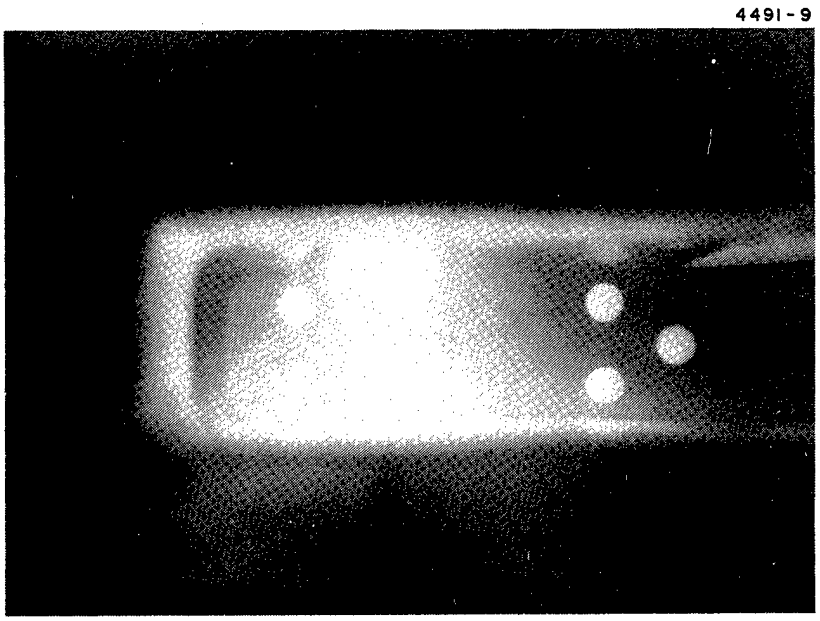

(b)

Fig. 25. Time exposed photographs of e-beam irradiated plasmas. (a) Pure helium flow. (b) Electrode streams contain Ar:He:1:30, laser flow contains F_2:He = 1:30 at 100 Torr.

Typical oscilloscope traces of e-beam current and sustainer voltage and current for cavity pressures of 100 Torr are shown in Fig. 26. The e-beam was turned on approximately 25 msec after the cavity pressure reached 100 Torr, remained on for approximately 55 msec, and fell to zero within approximately 20 msec. The ripple on the current trace is largely due to 60 Hz radiation pickup on the current transformer used to measure the current supplied by the high voltage power supply. The current trace also shows linear decay during the 55 msec on-time, but this was caused by the poor frequency response of the current transform to pulse lengths ≥1 msec signals. Calibration of the transform shows that the current actually remains constant to within ±5%.

The sustainer voltage is applied approximately 15 msec after the e-beam is turned on, remains on for approximately 55 msec, and falls to zero with a time constant of 200 msec. The electrode voltage for this test was a maximum of 4.2 kV at the beginning of the run, falling to 3.7 kV when the "crowbar" was applied to the storage capacitors. The current trace shows that electrode current flow begins when the electrode voltage is applied and remains nearly constant at 440 mA until the e-beam is turned off (the electrode current is measured using a current transform which is identical to the one used to measure e-gun current, and therefore exhibits a similar response to long pulses). After the e-beam is turned off, the current begins to fall to zero with approximately the same decay time as the e-beam current. Once the crowbar is turned on the electrode current decreases rapidly (≅5 msec) to zero.

The electrode current varies almost linearly with applied field over the range of field strengths investigated. Electrode current versus plasma voltage (electrode voltage minus voltage drop resistive electrode) is plotted in Fig. 27 for a cavity pressure of 100 Torr, and for an e-beam current density J_{eb} = 0.35 to 0.40 mA/cm^2. For both the 3% and 1.5% F_2/He mixtures, the plasma resistance is approximately 9 KΩ for the above J_{eb}. The variation of electrode current

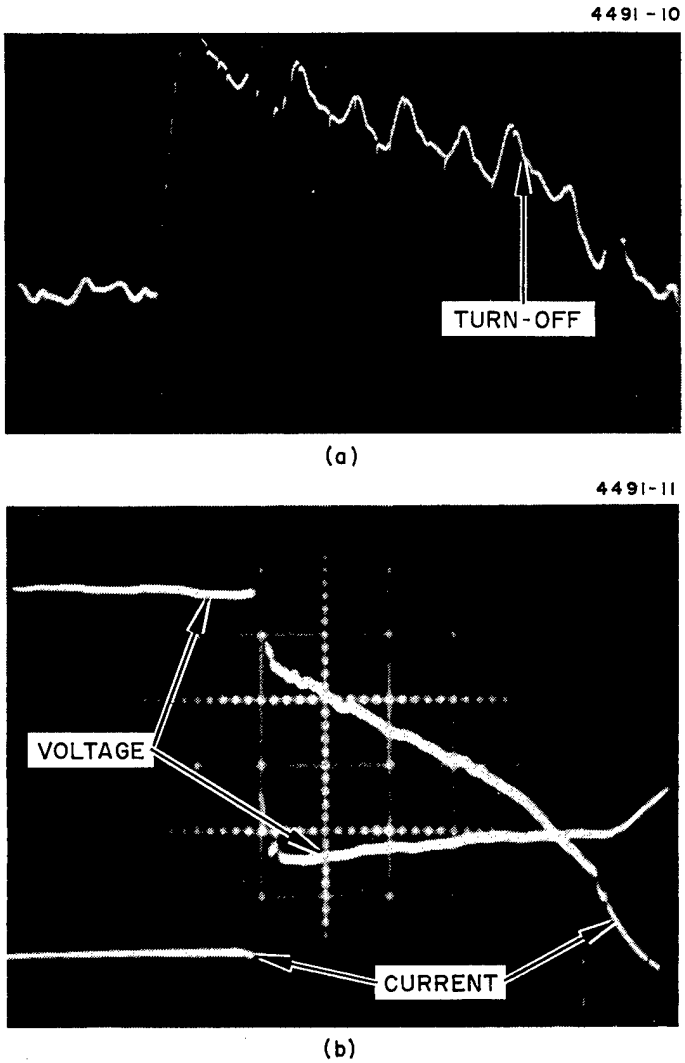

Fig. 26.
Typical e-gun current and discharge voltage and current records for F_2:H_2:He = 1:1:30, 100 Torr. Note: The current droop in both traces is due to poor response of the current transformer at low frequencies and not to a decrease in current. (a) E-beam current density oscillograph (vertical sensitivity, 0.125 mA/cm^2; sweep speed, 10 msec/div). (b) Electrode voltage and current oscillograph voltage (vertical sensitivity, 1 kV/div; sweep speed, 10 msec/div). Current (vertical sensitivity, 100 mA/div).

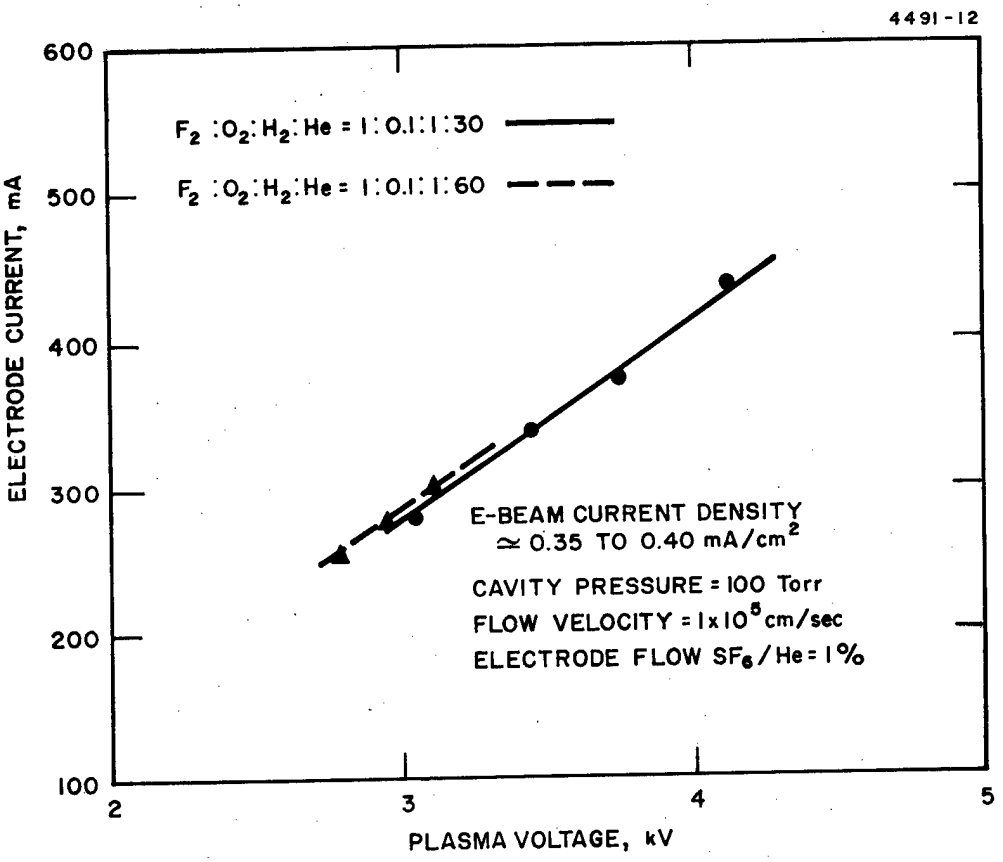

Fig. 27. Current-voltage characteristics of F_2:H_2:He mixtures, 100 Torr; Mach number ≃1.5.

with e-beam current density for a fixed electrode voltage of 3.5 kV is shown in Fig. 28. The results show the current (or plasma resistance) to be linear with J_{eb} according to eqs. (8) and (9). When $J_{eb} = 0$ we obtained no measurable current flow. If the electric field strength was too high and no e-beam was present, arcing would occur between the electrodes. This occurred for electrode voltages above 4 kV when the cavity pressure was 100 Torr.

The plasma voltage and current characteristics for a cavity pressure of 200 Torr are shown in Fig. 29. The results are similar to those found at 100 Torr, except the electrode voltage is increased to maintain a constant E/P. The plasma resistance has increased to approximately 17 kΩ and the current has remained nearly constant for a fixed E/P as we predicted in Section II-B-3. The results of J_s versus J_{eb} at 200 Torr in Fig. 30 again show the plasma resistance to be a linear function of e-beam current density J_{eb}.

A typical voltage and current record and a time-exposure photograph of the discharge at 200 Torr are shown in Fig. 31. The voltage and current traces are very similar to those at 100 Torr, with the current remaining constant while the e-beam current and electrode voltage are present. The photograph of the discharge is characteristic of non-self-sustained discharges with the region between the electrodes dark and the area surrounding the electrodes illuminated by the transition from a uniform discharge to an arc. In all our tests we observed the illumination near the anode (resistive electrode) to be concentrated at the downstream portion of the electrode. Since the drift velocity of plasma ions for large E/P's is comparable to the gas flow velocity,[5] the ion density or ion current will be larger downstream. The discharge photograph shows that most of the current density is concentrated at the downstream edge of the electrode.

Electrode current as a function of J_{eb} for cavity pressures of 300 and 400 Torr is plotted in Fig. 32. The current characteristics are again similar to those found at 100 and 200 Torr. The total maximum discharge current is approximately 500 mA, which corresponds

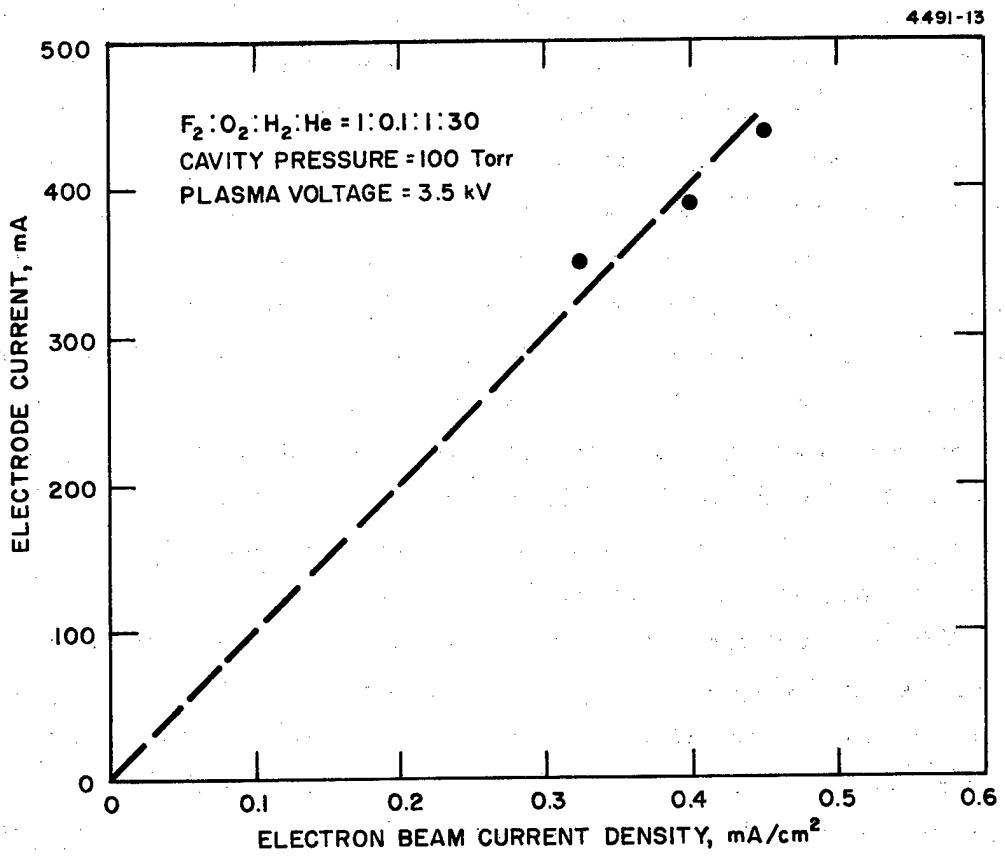

Fig. 28. Electrode current versus e-beam current density for F_2:H_2:He mixtures, 100 Torr; Mach number ≈1.5.

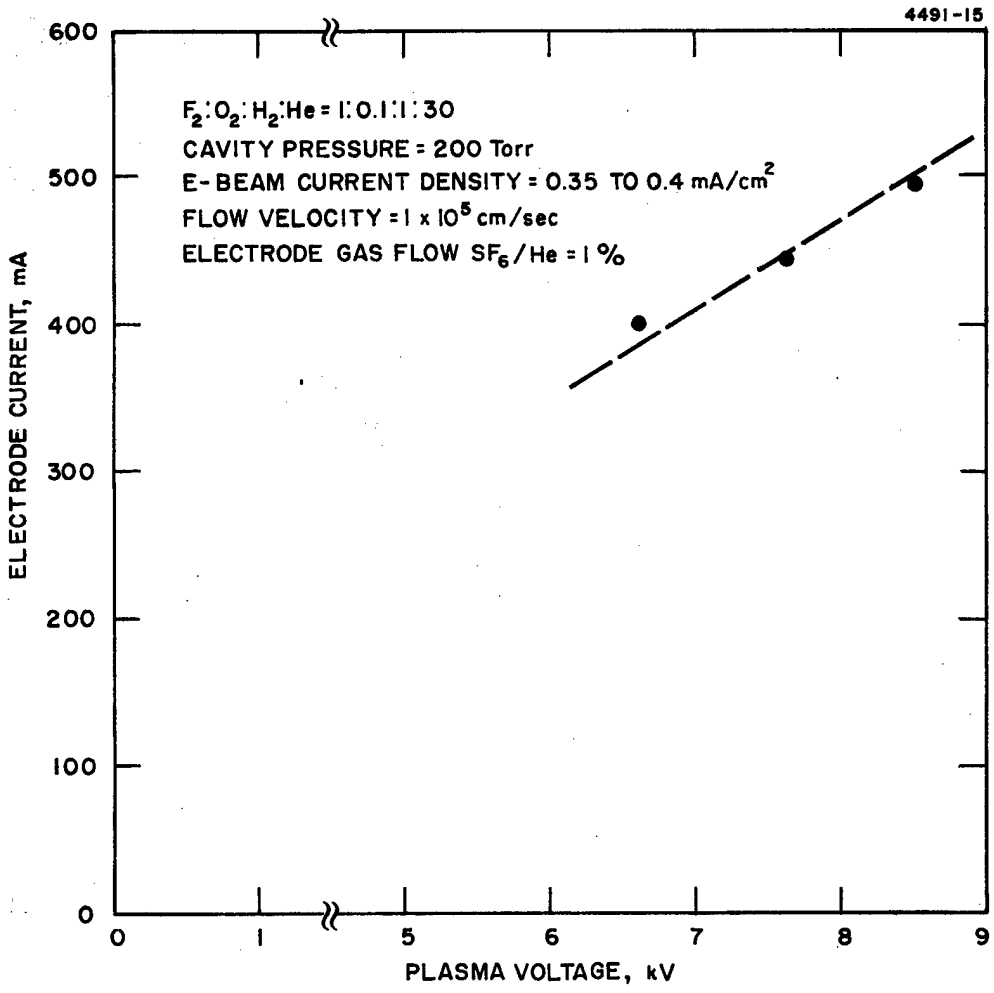

Fig. 29. Current-voltage characteristics of F_2:H_2:He mixtures, 200 Torr; Mach number ≃1.5.

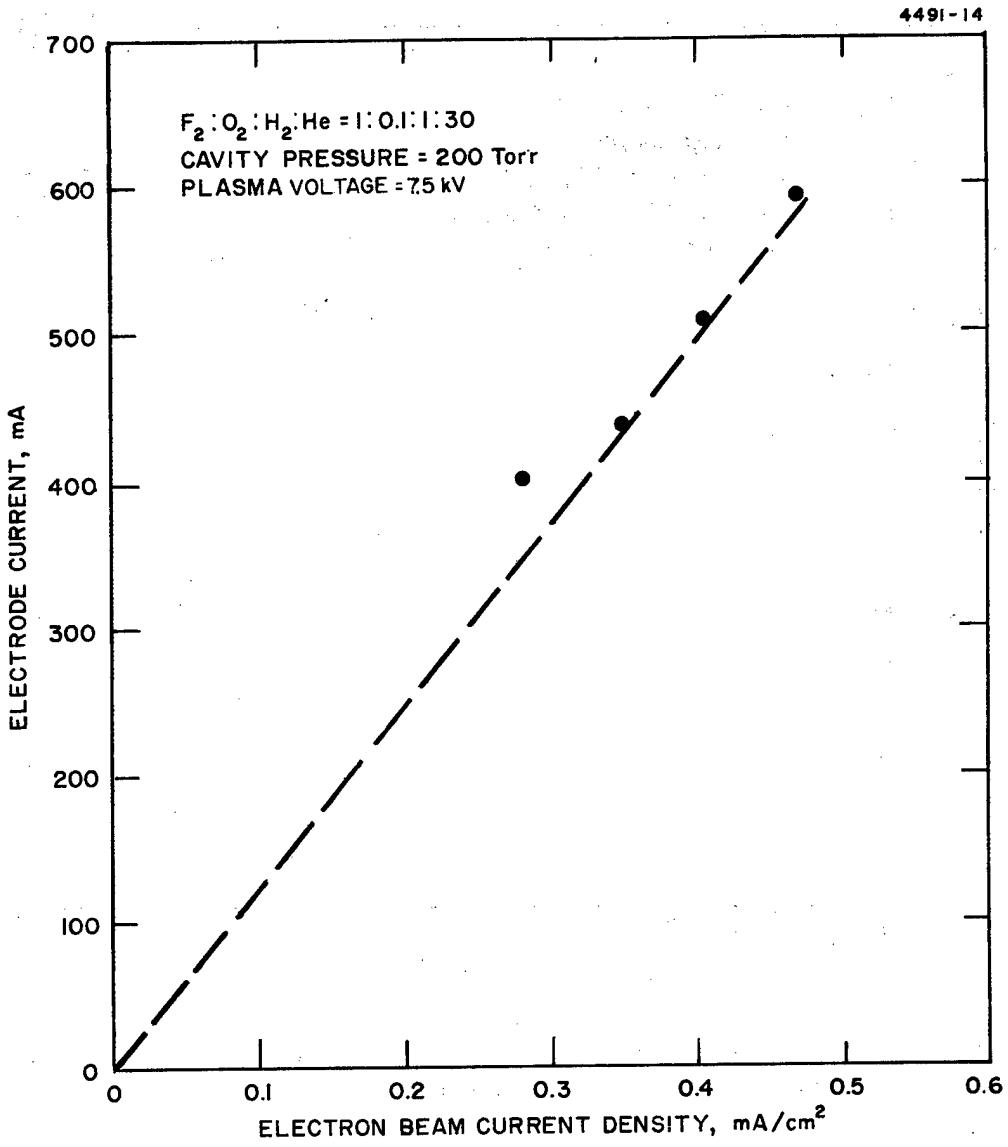

Fig. 30. Electrode current versus e-beam current density for F_2:H_2:He mixtures, 200 Torr; Mach number ≈ 1.5.

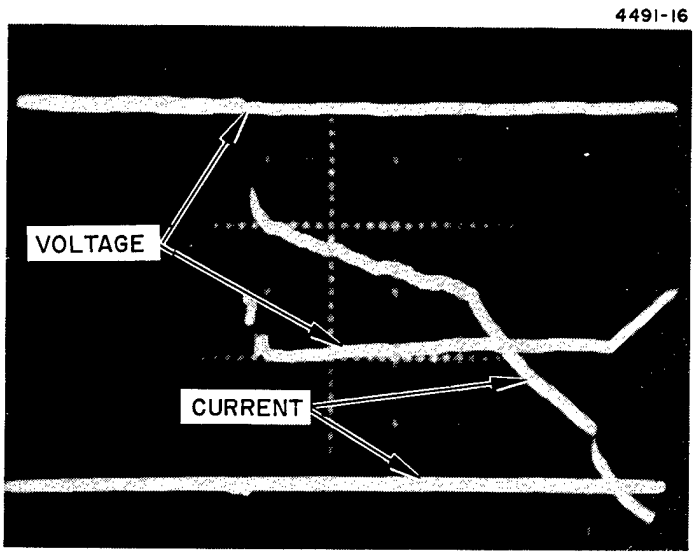

(a)

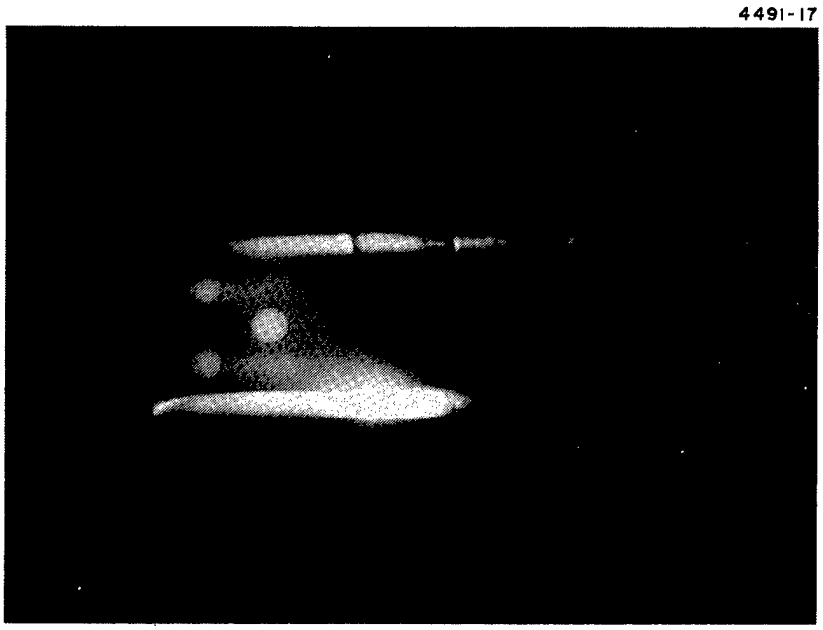

(b)

Fig. 31.
Typical current and voltage and photographic records for F_2:H_2:He = 1:1:30, 200 Torr. (a) Electrode voltage and current oscillograph. Voltage (vertical sensitivity, 2 kV/div; sweep speed, 10 ms/div). Current (vertical sensitivity, 100 mA/div), J_{eb} = 0.35 mA/cm^2. (b) Time exposed photograph of e-beam sustained discharge, F_2:H_2:He = 1:1:30, 200 Torr.

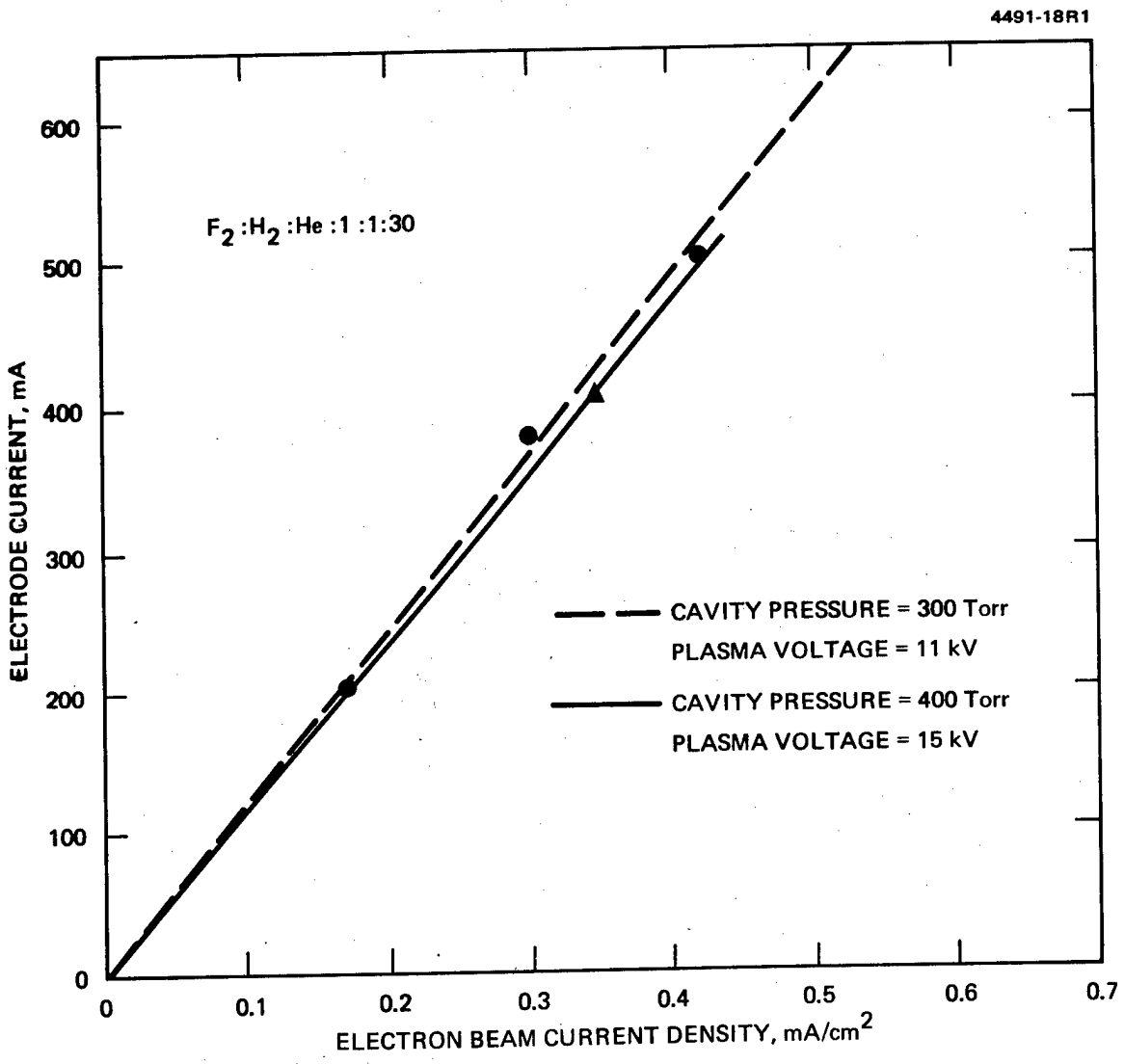

Fig. 32. Electrode current versus e-beam current density for F_2:H_2: He mixture, 300 Torr and 400 Torr; Mach number ≈1.5.

to approximately 60 mA/cm^2 if we assume that the discharge is uniformly distributed in the discharge region.

To measure the increase in stagnation temperature due to the chemical reaction, a fast response ($T \simeq 10$ msec) thermocouple was placed in the flow approximately 10 cm downstream from the discharge electrodes. It was anticipated that, at this location, the temperature would be near 800-900°K for a mixture F_2:H_2:He = 1:1/2:30, and a dissociation percentage $\alpha_s \simeq 0.2$ to 0.3%. However, for all discharge conditions reported above and at cavity pressures from 100 to 400 Torr, no temperature rise was measured except for the rise caused by the heat from the electrical discharge. At this point, several possibilities for the absence of a measurable chemical reaction were postulated: (1) the discharge current measured in the cathode lead was not a measure of the current between the two electrodes (e.g., some of the cathode current could be going downstream to the grounded dump tank); (2) the theoretical chemical reaction rate assumed in our calculations was not accurate for cavity temperatures of 175°K; (3) the effect of oxygen at low temperatures overstabilized the mixture, causing too slow a reaction rate for the cooled supersonic flow; and (4) the input power to the electrical discharge was not effective in dissociating a sufficient amount of the fluorine (e.g., the discharge current consists mainly of ion current). To determine if any of the above were responsible for the absence of any observable chemical reaction, several experiments and analytical calculations were performed.

To determine if the current measured in the cathode lead was actually flowing across the discharge region to the grounded e-gun foil which serves as the anode, all the ground returns for the e-gun were passed through a current transform similar to the one used to measure the current in the cathode lead. Several discharge measurements were made and in each case the measured current was identical for both transformers. Since all the discharge current is flowing between the two electrodes, the first possibility given above can be eliminated.

To determine if the chemical reaction rate could be increased, tests were performed using mixtures containing 6% fluorine and hydrogen. For a fixed amount of atomic fluorine produced by the discharge, the resulting chemical reaction rate will be twice that for the standard mixtures containing 3 percent fluorine and hydrogen. Several tests were run at 400 Torr for different combinations of discharge voltage and e-beam current density. The largest input power corresponded to a discharge voltage and current of 22 kV and 800 mA, respectively. This input power corresponds to an $\alpha_s \simeq 0.2\%$ if we assume the discharge current consists largely of electron current. Again, however, no chemical reaction was detected.

At this point we decided to investigate the effects of O_2 on the chemical reaction rate, since this had not been included in our previous calculations. It is conceivable that the minimum O_2 concentration needed to stabilize the mixture at room temperature will overstabilize the mixture when it is accelerated to Mach number $M \simeq 1.5$ and the gas cools to approximately $175^{\circ}K$. The following rates were added to our HF/DF kinetics code

$$H + O_2 + M \xrightarrow{K_H} H O_2 + M$$

where

$$K_H = 1 \times 10^{-33} \exp(800/T)\ Cn\ ,\ C_{He} = 1.0\ ,\ C_{F_2} = 3.0 \quad (10a)$$

and

$$F + O_2 + M \xrightarrow{K_{F_2}} F O_2 + M$$

where

$$K_{F_2} = 2\,KH_2 \tag{10b}$$

The time for one reaction step in Eq. (10b) and for one step of the hot reaction is plotted in Fig. 33 as a function of cavity pressure. For cavity pressures near 400 to 500 Torr, the hot reaction rate which produces F atoms is approximately equal to the attachment rate of F atoms by O_2. This result definitely explains why no chemical reaction would be observed at higher pressures in the presence of oxygen. However, since attachment by O_2 is a three body process, its reaction rate decreases with the square of the pressure while the hot reaction rate decreases linearly with pressure. Therefore, it should be possible to minimize the effects of overstabilization by O_2 in the cavity by operating at lower pressures.

Extensive tests were conducted at a pressure of 200 Torr to determine if lower cavity pressures would enhance the chemical reaction rate. Mixtures containing 3, 6, and 10 percent F_2 were investigated. Prior to electrical discharge tests, stability runs were made to determine the minimum O_2 concentration necessary to prevent prereaction in the subsonic mixer. The percentage of O_2 with respect to the F_2 concentration required was 2.5, 5, and 6%, respectively. For mixtures containing 10 percent F_2, the maximum discharge voltage was approximately 15 kV. Higher voltages could be reached if the e-gun was not turned on. At voltages above 15 kV, an arc would occur downstream along the lower teflon channel wall when the e-gun turned on. It is believed that the higher energy electrons from the e-gun strike the teflon and charge the dielectric to a voltage comparable to the cathode discharge electrode. This effectively causes the cathode to extend downstream toward the grounded dump tank. At some point along the teflon surface, the voltage will reach a value where surface breakdown will occur. This breakdown mode determined the maximum discharge voltage for all our test runs.

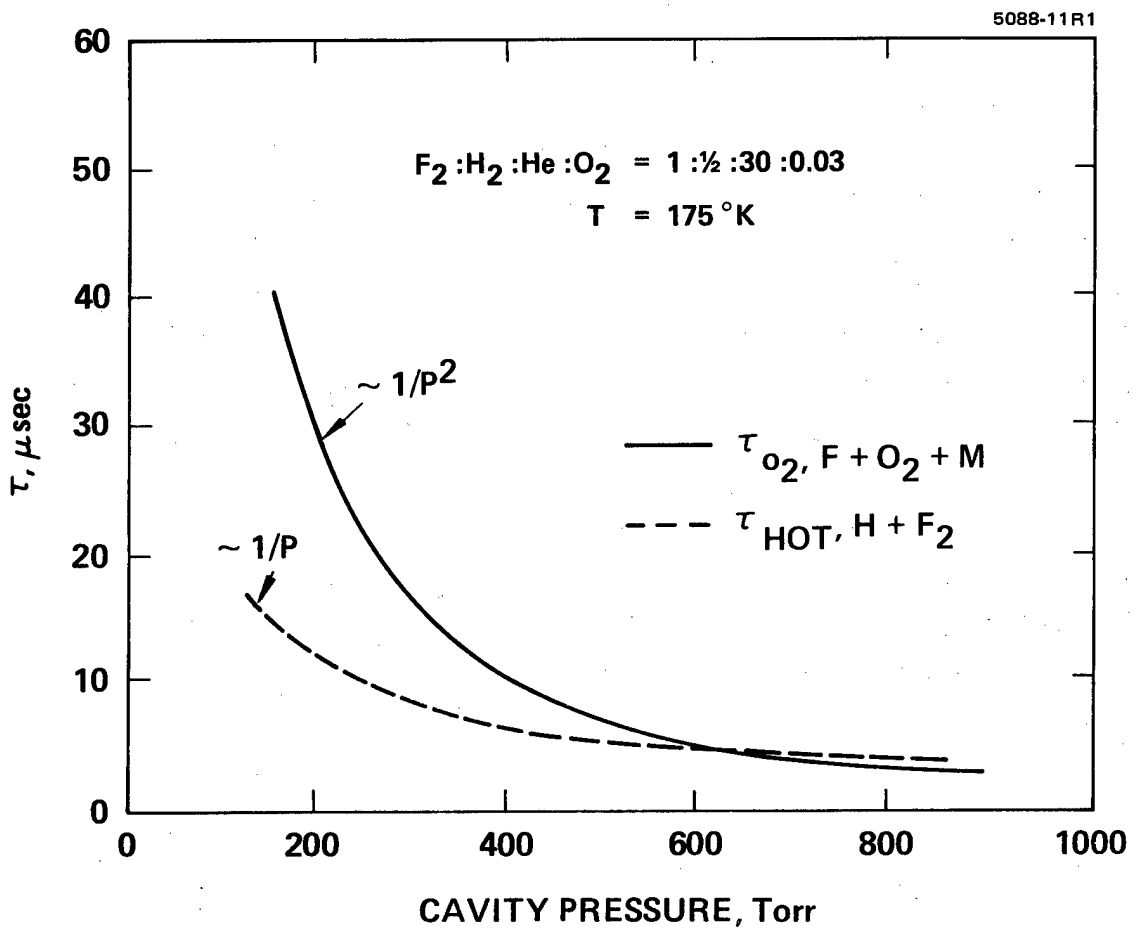

Fig. 33. Comparison of reaction rates for various pressures, Mach number ≈1.5.

Figure 34 gives the discharge voltage-current characteristics for a mixture containing 3 and 10 percent F_2. The results show that for a given discharge voltage and e-beam current density J_{eb}, the discharge current depends strongly upon the F_2 concentration. At first it was believed that the dependence of discharge current J_s on F_2 concentration was due to the increased dissociative attachment rate for the process $e + F_2 \longrightarrow F + F^-$. However, results from our discharge code for the $H_2/F_2/He$ system, which are presented in Section V, indicate that the mobility of the charge carriers decreases with increasing F_2 concentration and therefore cause the current to decrease for a given discharge voltage. Thermocouple data obtained for all three mixtures tested were the same as before, with no observable chemical reaction.

The above tests indicated that overstabilization by O_2 was not the problem; however, uncertainty concerning effect of gas cooling on O_2 and on chemical reaction rates still remained. To eliminate the temperature uncertainty, it was decided to remove the three expansion nozzles in the flow channel and convert the full channel to subsonic flow. For Mach numbers $M \simeq 0.7$ to 0.8 the flow temperature should be approximately $260^{\circ}K$ at the entrance to the cavity. In the following section these subsonic flow experiments and theoretical predictions relating to the lower Mach number flow are discussed.

B. Subsonic Flow

The most dramatic effect noted in going to subsonic flow is seen in Fig. 35 where the time for one reaction step in Eq. (10b) and for one step of the hot reaction is plotted for $T = 260^{\circ}K$. For supersonic flow conditions the two reaction times were almost identical at 400 to 500 Torr (see Fig. 33), but for subsonic flow conditions the hot reaction time was approximately two orders of magnitude larger; therefore, the effect of O_2 on the chemical reaction should be minimal. For further comparison with supersonic flow predictions, the calculated

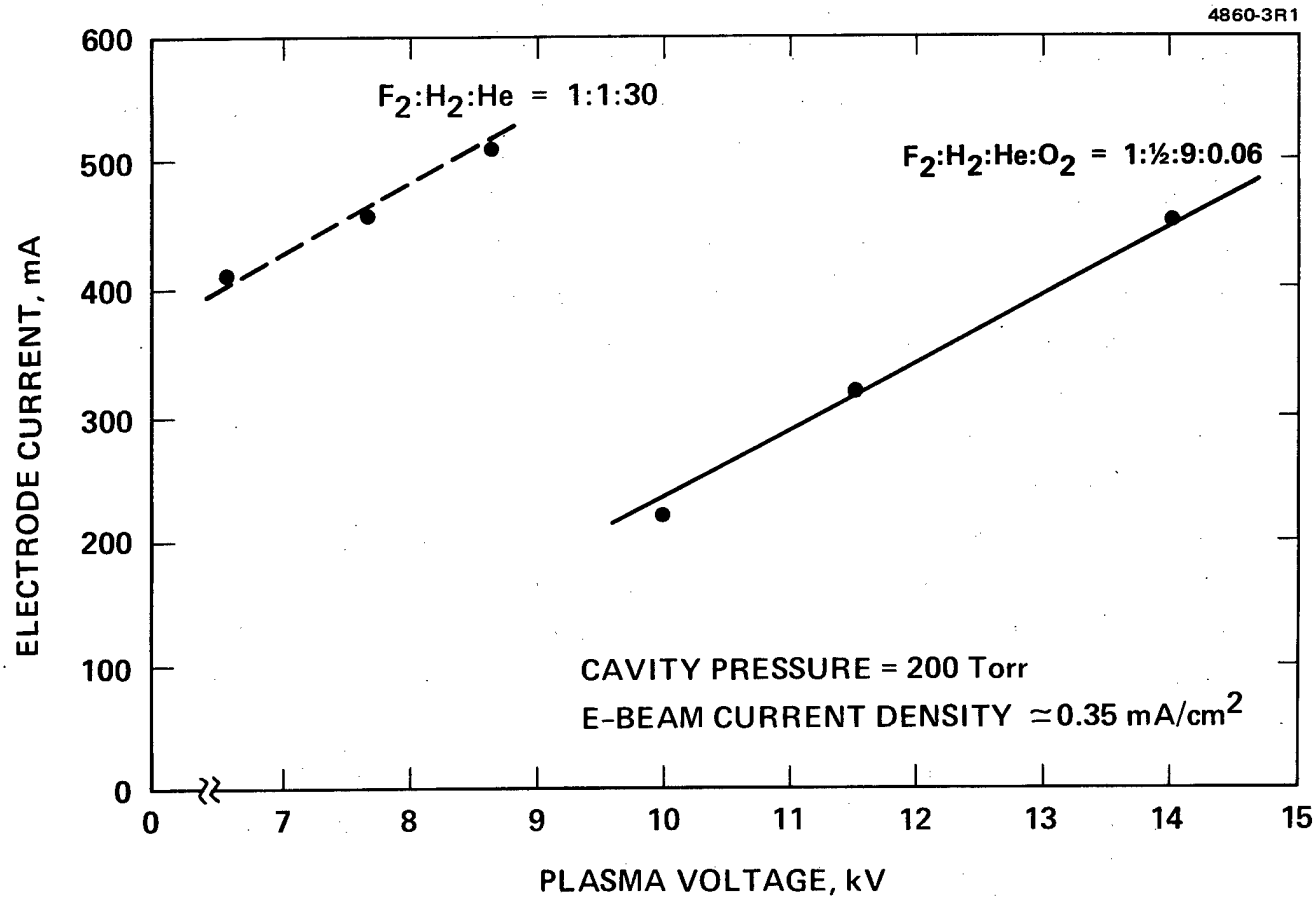

Fig. 34. Current-voltage characteristics of 3% and 10% F_2 mixtures, 200 Torr; Mach number ≃1.5.

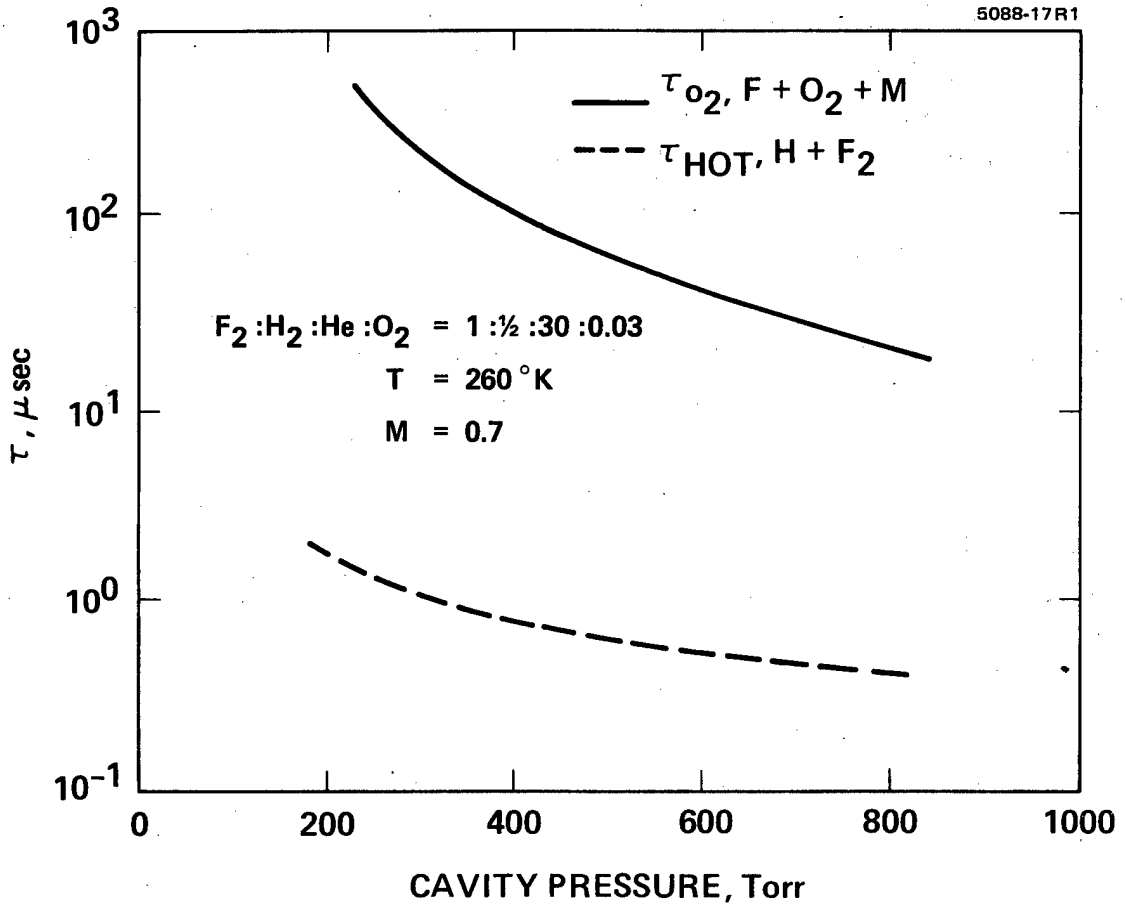

Fig. 35. Comparison of reaction rates for various pressures, Mach number = 0.7.

lasing zone length and specific power for M = 0.7 are plotted in Figs. 36 and 37, respectively. It should be noted that there is significant improvement in specific power for subsonic flow conditions. This is a result of faster chemical reaction rates due to the higher initial cavity temperature. These predicted results show that if the higher cavity temperatures enhance the chemical reaction rate to the point where the electrical discharge will be effective, no laser degradation is expected. What would occur, however, is a loss in pressure recovery because of the lower Mach-number flow. The maximum pressure recovery would be approximately the static cavity pressure.

Subsonic flow was achieved in the demonstration device by removing the supersonic nozzle block and allowing the laser gas mixture to fill the entire 2 x 6 cm^2 flow channel. The flow ducts which brought the He/SF_6 electrode purge gas into the nozzle block were sealed and the area which housed the nozzle block was made to form a smooth transition into the flow channel. The gas flow rate in the cavity was controlled by storage tank pressure and upstream orifice plates, and the cavity pressure was controlled by the initial pressure in the dump tank. For example if we wanted a cavity pressure of 400 Torr for a subsonic flow run, the dump tank was filled with air to 400 Torr prior to the run.

Approximately ten subsonic runs were made at a cavity pressure of 400 Torr, mixtures of $F_2:O_2:H_2:He$ = 1:0.03:1/2:30, and flow Mach number M ≃ 0.6. Figure 38 shows the discharge current density for a discharge voltage = 6.0 kV. The electrode current varies linearly with J_{eb}, but is considerably less than the current obtained for the same mixture and pressure at supersonic flow conditions (see Fig. 32). The reason for this is the lower breakdown voltage between the cathode and the downstream dump tank. The downstream arc would not form until the e-gun was turned on and discharge current started to flow. The maximum voltage obtained without breakdown was approximately 9 kV compared to 22 kV for supersonic conditions. The lower breakdown voltage is partially due to warmer subsonic gas flow,

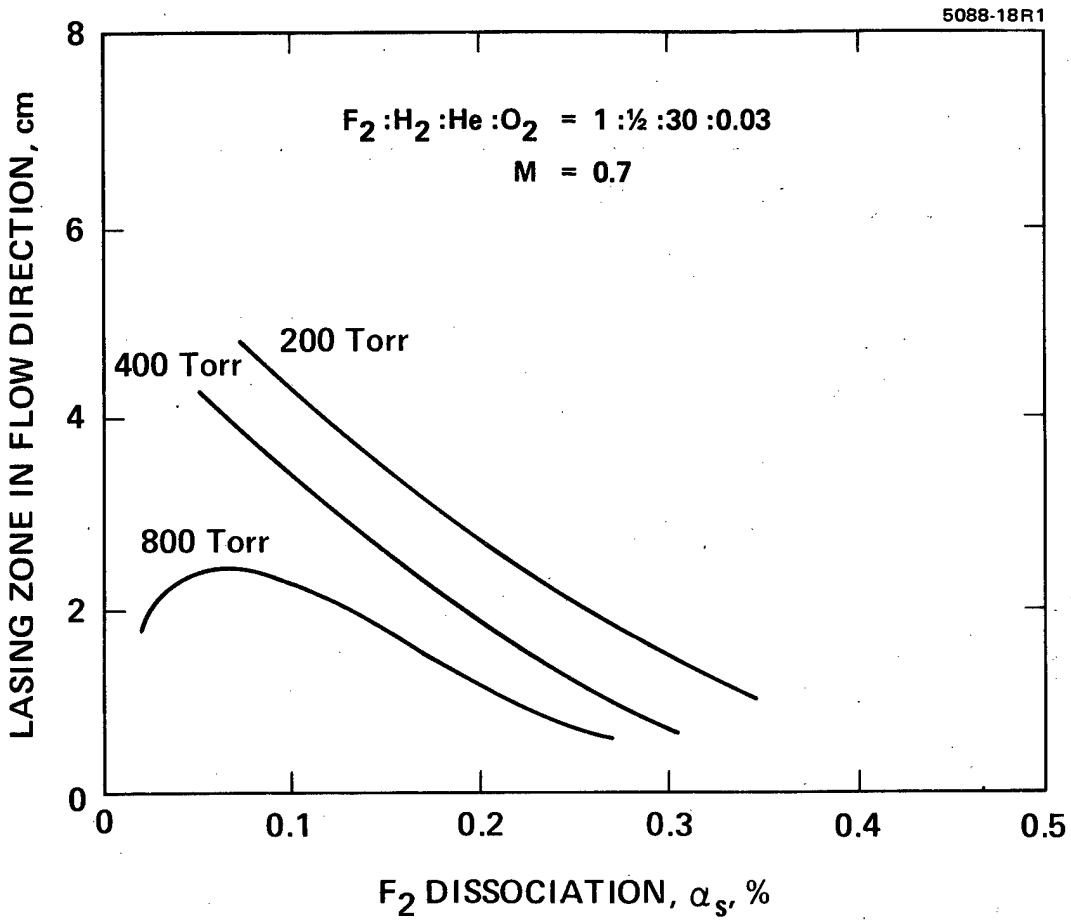

Fig. 36. Predicted lazing zone versus cavity pressure and fluorine dissociation, Mach No. = 0.7.

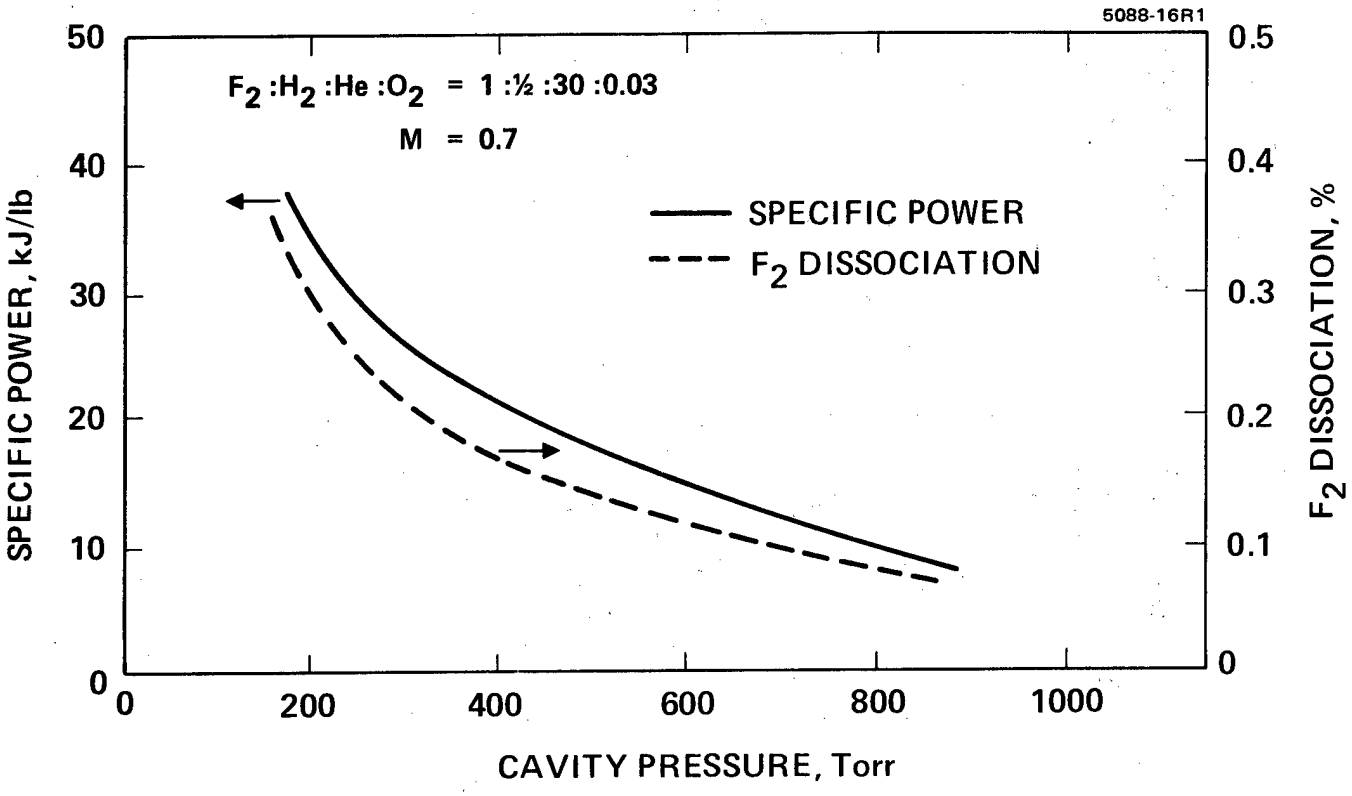

Fig. 37. Predicted laser performance versus cavity pressure, Mach Number = 0.7.

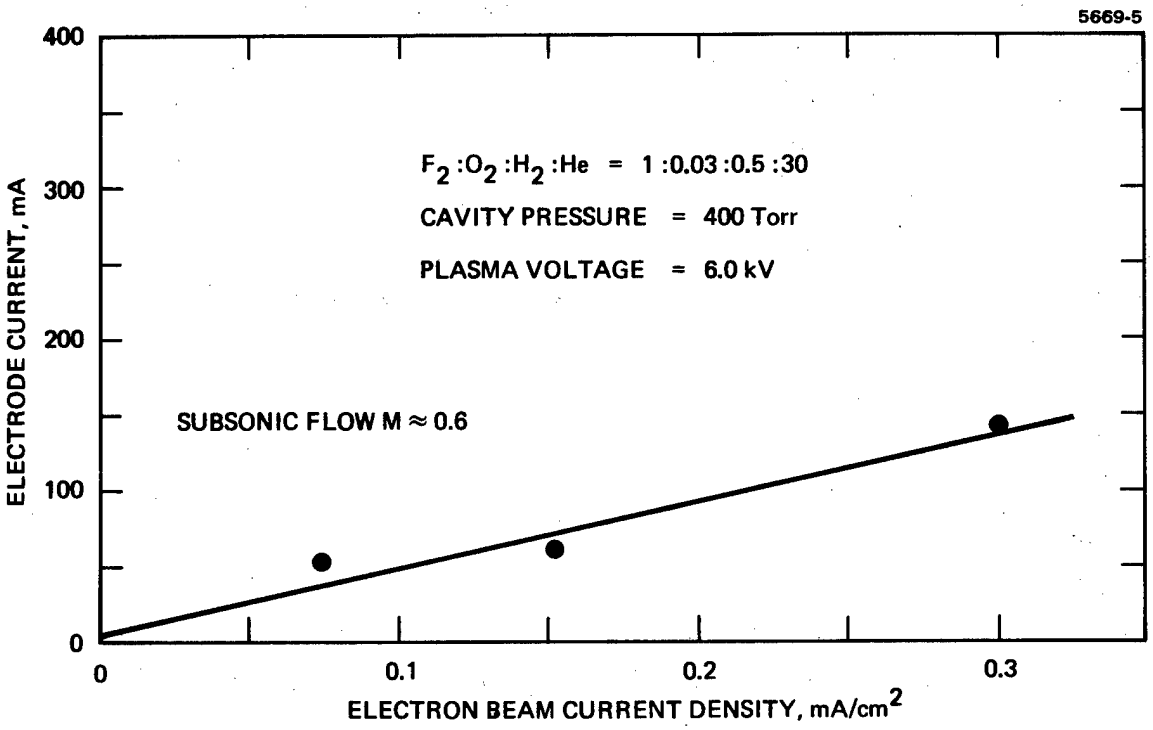

Fig. 38. Electrode-current versus e-beam current density for F_2:H_2: He = 1:1/2:30 mixture, 400 Torr; Mach number ≈0.6.

resulting in lower gas density for a given cavity pressure. Also, the effect of the lower gas velocity over the teflon channel wall probably has an important part in determining surface breakdown voltages. For voltages below breakdown, the electrode current given in Fig. 38 is in very good agreement with the electrode current given in Fig. 32 if the latter is reduced proportionally to the difference in E/ρ for the two experiments. This is consistent with the voltage-current characteristics for supersonic flow conditions which were presented earlier.

The thermocouple results for both 300 and 400 Torr cavity pressures again showed no indication of any chemical reaction initiated by the electrical discharge. This result eliminates overstabilization by O_2 as the total cause for the absence of any initiation. Since we have eliminated improper discharge current paths, O_2 stabilization, and gas temperature effects as causes, only one possibility remains from the four suggested in Section IV-A: the electrical discharge is ineffective in dissociating F_2. In Section V we present the results of a computer code which treats fluorine dissociation in an e-beam sustained electrical discharge. The results presented strongly suggest that, because of the large electron attachment rate, the measured electrode current is over 90 percent ion current. This results in too low an electron density and a fluorine dissociation fraction which is too low for efficient initiation.

V. E-BEAM SUSTAINED DISCHARGE ANALYSIS IN F_2/He/Ar MIXTURES

E-beam sustained F_2/He/Ar discharges are analyzed under the following assumptions: (1) space charge separation and diffusion are neglected, (2) gas heating is negligible, and (3) all electron-ion pairs are generated by the e-beam. The reaction and rate constants considered in the plasma model are

$$Ar + e_f \longrightarrow Ar^+ + e + e_f \qquad S_{Ar} = 1.0 \text{ ion pairs/cm torr} \qquad (12)$$

$$He + ef \longrightarrow He^+ + e + e_f \qquad S_{He} = 0.03 \text{ ion pairs/cm torr} \qquad (13)$$

$$F_2 + e_f \longrightarrow F_2^+ + e + e_f \qquad S_{F_2} = 0.3 \text{ ion pairs/cm torr} \qquad (14)$$

$$Ar^+ + F_2 \longrightarrow F_2^+ + Ar \qquad 2.4 \times 10^{-9} \text{ cm}^3/\text{sec} \qquad (15)$$

$$He^+ + F_2 \longrightarrow F_2^+ + He \qquad 1.7 \times 10^{-9} \text{ cm}^3/\text{sec} \qquad (16)$$

$$F_2 + e \longrightarrow F + F^- \qquad 2 \times 10^{-9} \leq K_{DA} \leq 2 \times 10^{-7} \text{ cm}^3/\text{sec} \qquad (17)$$

$$F_2^+ + F^- \longrightarrow 3F \qquad 4 \times 10^{-8} \text{ cm}^3/\text{sec} \qquad (18)$$

$$F^- + M \longrightarrow F + e + M \qquad 0 \leq K_{DET} \leq 4 \times 10^{-12} \text{ cm}^3/\text{sec} \qquad (19)$$

All the above rates were taken from Refs. (6) and (8).

Reactions (12) through (14) refer to the ionization of neutral gas species by high energy electrons. The volumetric rate of ionization of species i at partial pressure P_i is Q_i (ion pairs/cm^3 sec) = $S_i P_i J_{eb}/e$ = $4.7 \times 10^{21} J_{eb}(A/cm^2) P_i(atm) S_i$ (ion pairs/cm torr). Reactions (15) and (16) are the charge transfer processes from the ionized species to F_2. Reaction (17) is the dissociative attachment of slow electrons to

F_2 molecules. The fastest rate given comes from recent measurements in Ref. (9); the slowest rate showing, which is two orders of magnitude slower than any other, has been generally accepted as the attachment rate. Reaction (18) is the ion-ion recombination process and is an important F atom producer in electrical discharges. Reaction (19) refers to electron detachment by neutral molecules colliding with F^- atoms. This process, as we will see, must be considered if our computer model is to accurately predict experimental results obtained from pulsed chemical lasers.

To check the accuracy of our discharge model, we compared predicted results for electrode current and fluorine dissociation percentage with experimental results for a pulsed e-beam sustained chemical laser reported by Hofland et al.[10] Their discharge parameters were $J_{eb} \simeq 3$ A/cm^2, $\tau_{eb} = 50$ nsec, $J_s \simeq 7$ A/cm^2, and E/P = 11 kV/cm-atm, and optimum laser performance was obtained using a mixture of F_2:H_2:Ar:He = 6:3:37:54. The total electrode current was computed for the above conditions using the following expression

$$J_s = e\left(\mu_e \eta_e + \sum_i \mu_i \eta_i\right) E \qquad (20)$$

where μ is the mobility. We set $\mu_e = 500$ cm^2/V-sec and assume an average mobility for all ions $\bar{\mu}_i = 4.7$ cm^2/V-sec. Figure 39 shows the comparison between calculated and measured results. The computed current rises sharply during the time the e-gun is on and decays gradually in the afterglow period following the e-gun turn-off. The computed current is seen to closely approximate the measured results and is well within the experimental uncertainty for the parameters given above.

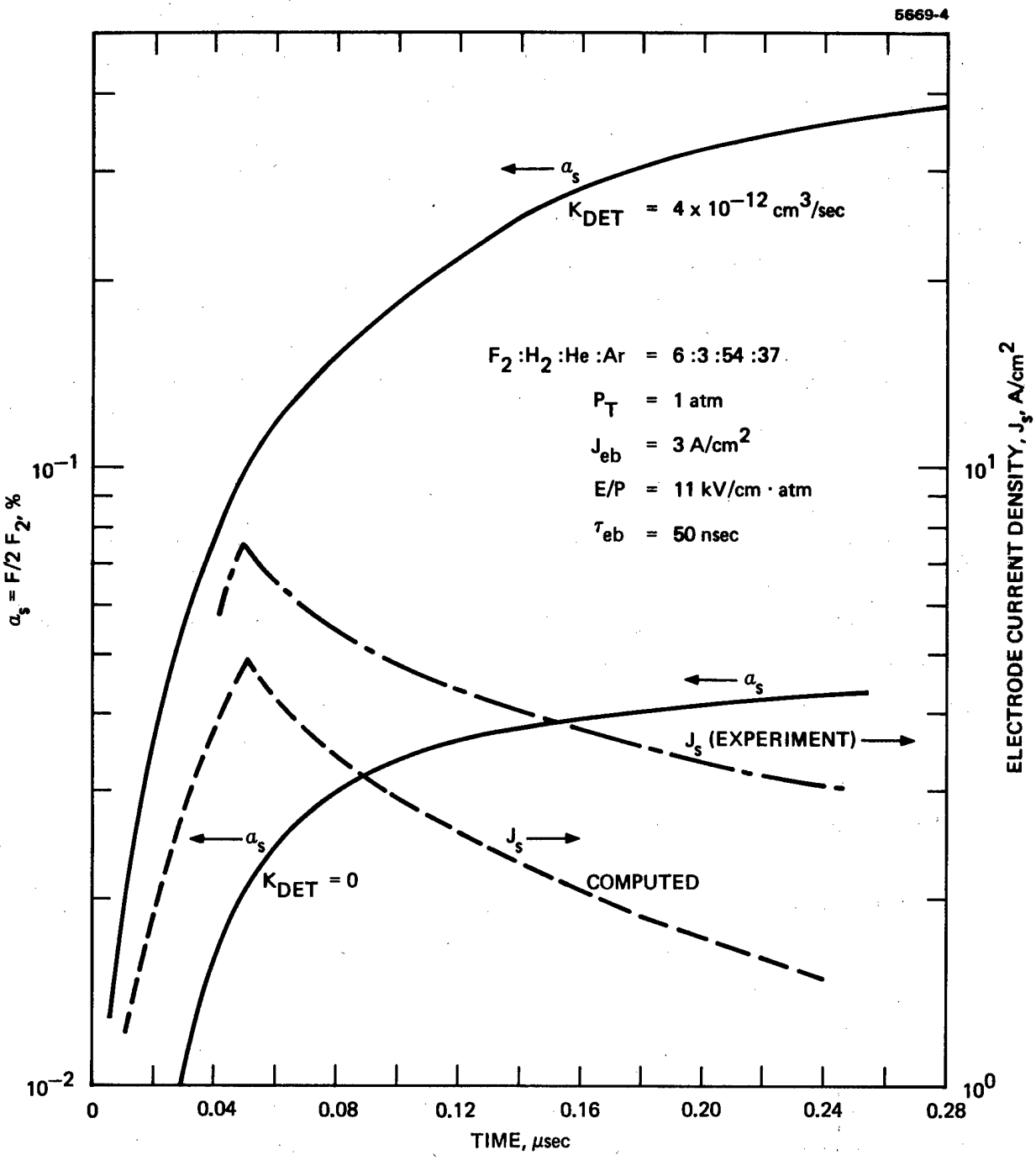

Fig. 39. Comparison of calculated electrode current density and fluorine dissociation with measured values reported in Ref. 8.

The calculated fluorine dissociation α_s has been plotted for two values of K_{DET}. For $K_{DET} = 4 \times 10^{-12}$ cm^3/sec, α_s approaches a constant value near 0.4 to 0.5%. This value is in agreement with a later report by Hofland et al.[8] The importance of electron detachment on α_s can be seen when α_s is plotted for $K_{DET} = 0$. The resulting dissociation is approximately an order of magnitude lower. Some insight can be gained by looking at the effect of K_{DET} on the charge carrier concentrations in Fig. 40. Ion carrier concentration F_2^+ and F^- are relatively independent of K_{DET}, while the opposite is true for the electron density η_e. For $K_{DET} = 0$, η_e is approximately an order of magnitude smaller than for $K_{DET} = 4 \times 10^{-12}$ cm^3/sec and falls rapidly to zero after e-beam burn-off. The latter accounts for the small contribution to α_s in the afterglow discharge. Also, since $\eta_e \ll F_2^+$ and F^-, J_s contains over 90 percent ion current and therefore is independent of K_{DET}.

Since the discharge model is seen to give reasonable agreement for the pulsed e-beam discharges, we used the computer code to analyze our cw e-beam discharge in the demonstration device. The basic differences between the two discharges are the magnitude of e-beam current density, J_{eb}, and length of e-beam pulse length, τ_{eb}. In the cw device, $J_{eb} \simeq 0.2$ mA/cm^2 as compared to $J_{eb} \simeq 3$ A/cm^2 for the pulsed device. For the cw device τ_{eb} is the transit time for the gas to flow across the electrodes. For the demonstration device $\tau_{eb} = 30$ μsec, which corresponds to a flow Mach number $\simeq 0.7$ and an electrode width = 2 cm. This is compared to $\tau_{eb} = 50$ nsec for the pulsed device.

Figure 41 shows the calculated current density J_s and fluorine dissociation α_c for the above two values of K_{DET}. Integrating the current density shown results in a total current of approximately 85 mA. This is in good agreement with measured values for the demonstration device given in Fig. 38. The calculated value for α_s is seen to rise to 0.09 percent for $K_{DET} = 4 \times 10^{-12}$ cm^3/sec, but is over two orders of magnitude lower for $K_{DET} = 0$. It should be noted that the amount

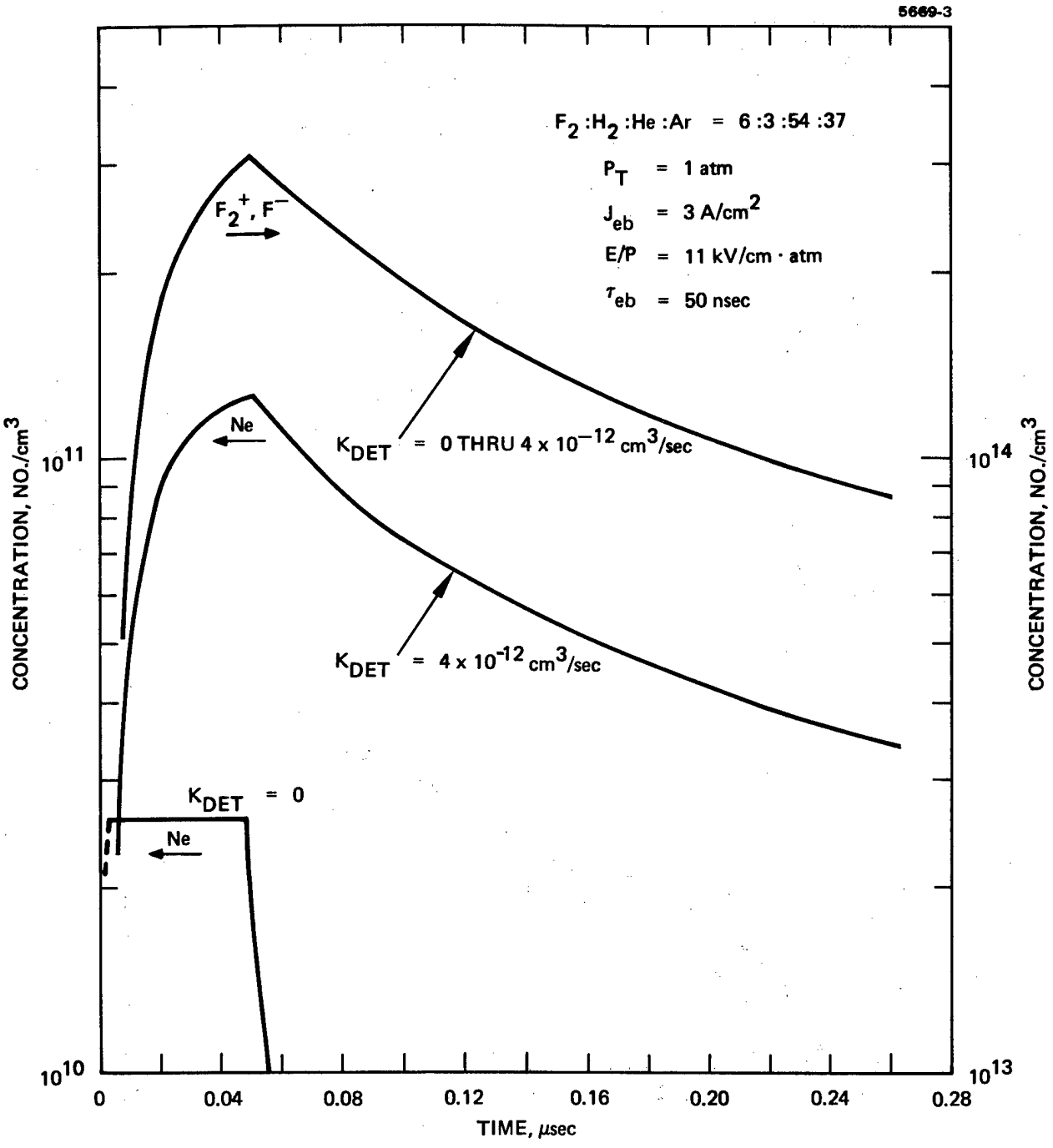

Fig. 40. Calculated charge carrier concentration for e-beam sustained discharge.

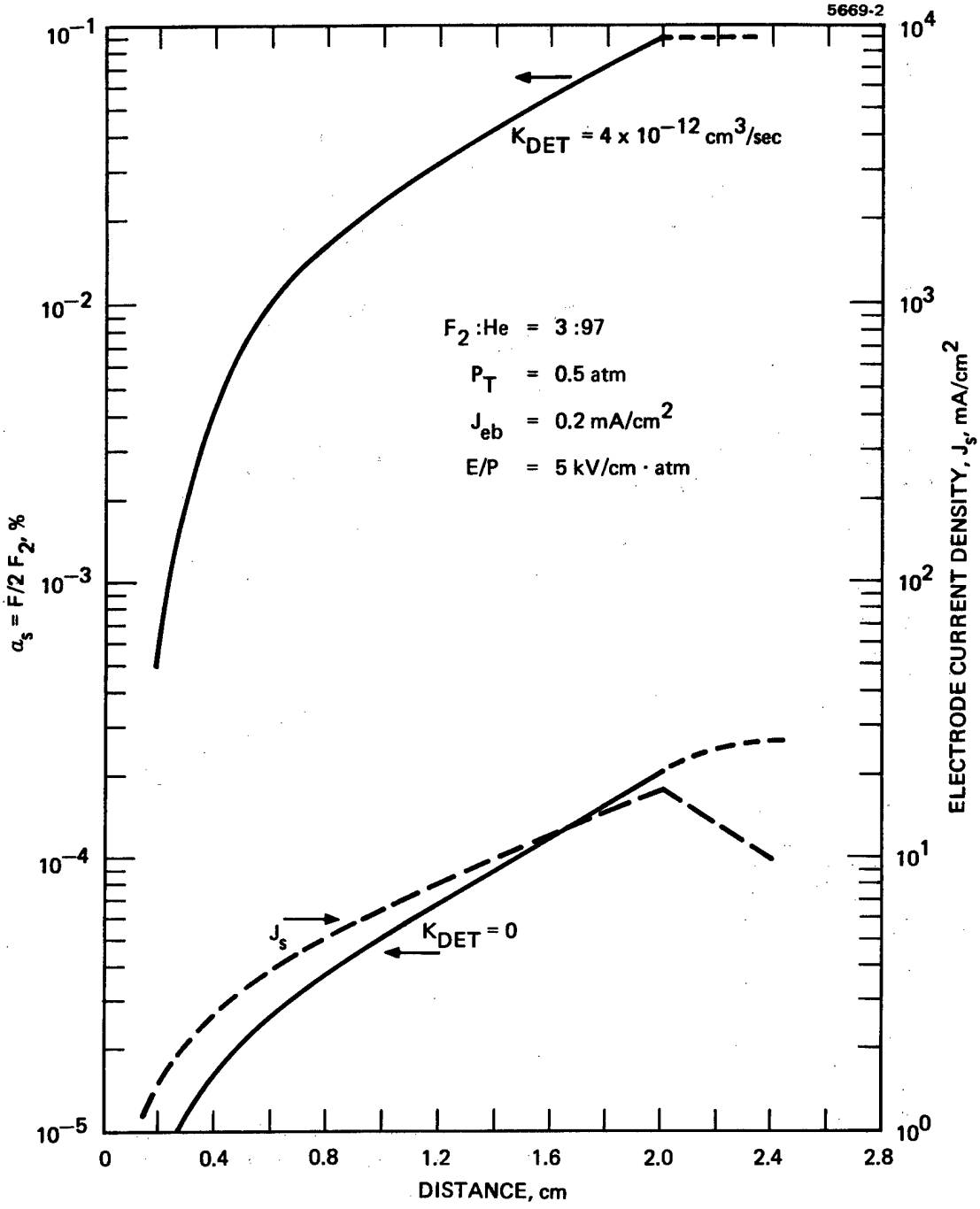

Fig. 41. Calculated electrode current density and fluorine dissociation for demonstration device, Mach number ≈0.7.

of dissociation has a much stronger dependence on the value of K_{DET} for low e-beam initiated devices than for the strongly initiated pulsed devices. This can be seen more clearly in Fig. 42, where η_e is plotted for the two values of K_{DET}. The electron concentration is three orders of magnitude less for $K_{DET} = 0$ than for $K_{DET} = 4 \times 10^{-12}$ cm^3/sec. This is to be compared to the results in Fig. 40 where the difference is less than one order of magnitude.

According to the results in Fig. 41, α_s should be sufficient to inititiate the chemical reaction if we assume $K_{DET} \simeq 4 \times 10^{-12}$ cm^3/sec. However, Mandel et al[11] have shown that K_{DET} depends on the temperature of the negative ion in the following manner

$$K_{DET} = \left(1.3 \times 10^{-10} T_i^{1/2} \exp(-4.2/T_i)\right) cm^3/sec \qquad (21)$$

where T_i is the temperature of F^- in electron units. Hofland[8] has shown that T_i is proportional to the square of the ion drift velocity V_d^2, where V_d is approximately proportional to E/P of the discharge. Since the discharge E/P of the demonstration device is approximately half that for the pulsed devices, the ion-drift velocity should be approximately 50 percent of the pulsed devices. This reduces the ion temperature 75 percent and according to Eq. (21) causes K_{DET} to decrease by over three orders of magnitude.

According to the above argument, we can assume $K_{DET} \cong 0$ for the demonstration device in the subsonic flow configuration, resulting in an α_s too low to initiate an observable chemical reaction. Since higher concentrations of F_2 were not used in the subsonic flow configuration, higher E/P's were not tried. It seems clear, however, that electron detachment is very important in low e-beam discharge devices. Therefore, discharge E/P's comparable to pulsed devices will be required. According to Fig. 41, a factor of two in the uncertainty in K_{DET} could mean failure or success by the electrical discharge to efficiently initiate a cw chemical laser.

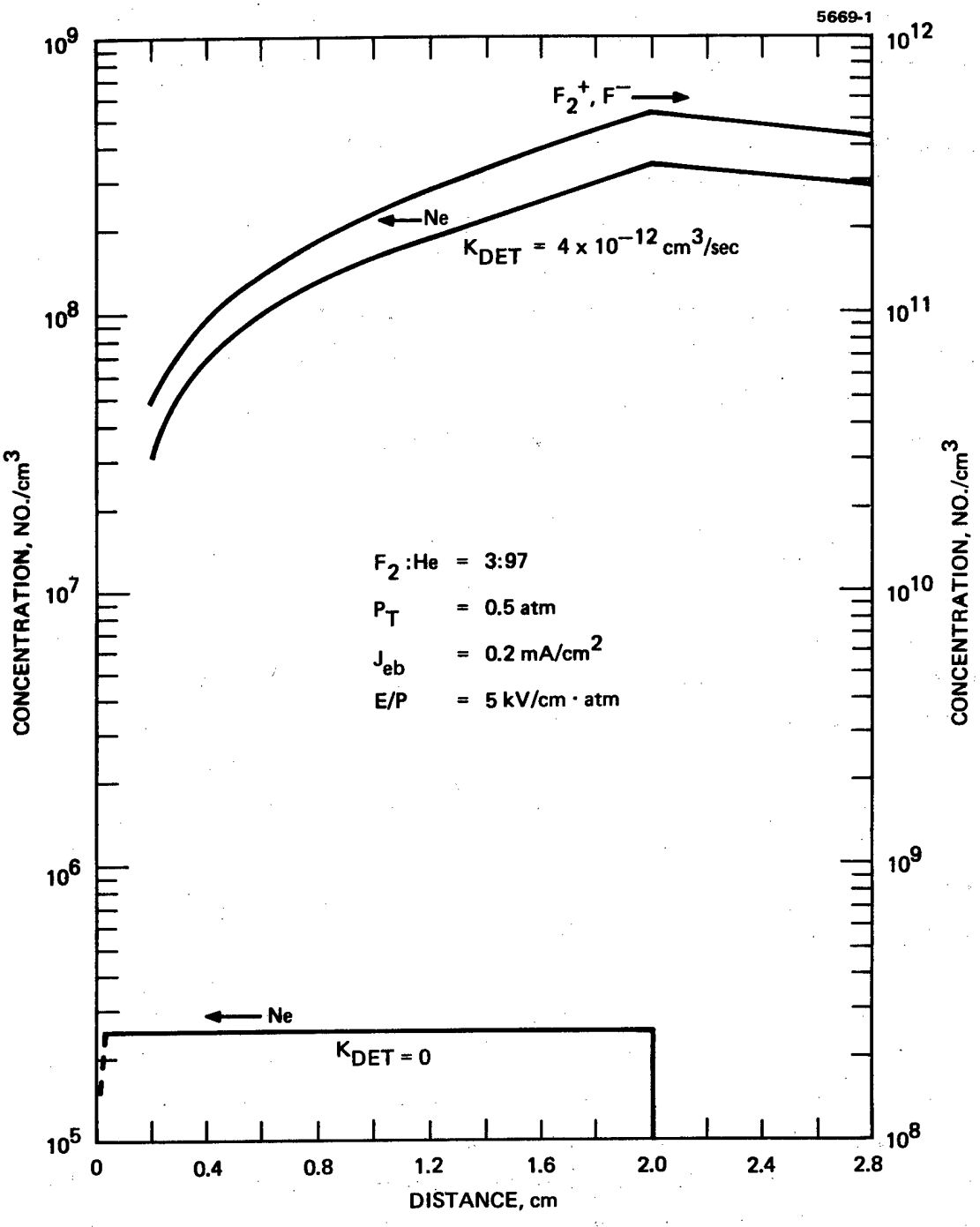

Fig. 42. Calculated charge carrier concentration for demonstration device, Mach number 0.7.

VI. SUMMARY

Based upon initiation difficulties experienced during the program, it appears that high-pressure, supersonic-flow, cw chemical lasers are not feasible. Because of gas cooling caused by supersonic flow, it appears that the oxygen used to stabilize the reactants as they mix "on the fly" in the room temperature subsonic mixer overstabilizes the gas mixture in the colder cavity. At cavity pressures above 0.5 atmosphere and temperatures near 175°K, the attachment rate of O_2 and F is believed to be faster than the hot reaction rate, thus causing any initial reaction to be quenched. It may be possible to find a substitute for O_2 which has an attachment rate independent of temperature; however, no investigation in this direction was performed during this program.

Overstabilization effects by the cold oxygen were eliminated during the program by reducing the gas flow to Mach number $M \simeq 0.7$ in the demonstration device. Analytical results showed that warmer cavity temperatures caused an improvement in specific power and electrical efficiency, but reduced the final recovery pressure. Experimental results showed that under subsonic flow conditions, the e-beam sustained discharge was not effective in initiating an observable chemical reaction. An electrical discharge kinetics code verified our findings by showing that for the discharge condition in the demonstration device, the fluorine dissociation fraction is several orders of magnitude below the value required for efficient initiation. The kinetics code showed that for low e-beam current densities such as those required for cw devices, the amount of dissociation is strongly dependent upon the detachment process $F^- + M \rightarrow F + M + e$, and that the rate at which electrons are produced depends upon the discharge E/P. The detached electron creates an atomic fluorine via associative attachment to F_2. For E/P's comparable to those obtained in atmospheric-pressure, pulsed chemical lasers, the detachment rate appears to be just sufficient to produce dissociation fractions necessary

for efficient initiation. However, in the demonstration device lower values of E/P were required to prevent breakdown between the cathode and a downstream ground. It appears that because ions in a cw device are swept downstream with the flow, electrode voltages must be below those values obtained in pulsed devices for similar gas mixtures and pressure to prevent voltage breakdown. The lower operating E/P causes a significant decrease in the detachment rate, causing insufficient atom fluorine production by the electrical discharge.

REFERENCES

1. A. H. Shapiro, The Dynamics and Thermodynamics of Compressible Fluid Flow, Vol. 1 (The Ronald Press Company, New York, 1953).

2. A. W. Ratliff, Lockheed Missiles and Space Company, Inc., Huntsville, Alabama.

3. D. B. Rensch, "Experimental Chemical Laser Mode Control," Final Technical Report, October 1974, Hughes Research Laboratories, Contract No. DAAH01-74-C-0596.

4. Jack Wilson, Hao-Lin Chen, Walter Fyle, and Raymond L. Taylor, J. Appl. Phys. Vol. 44, No. 12, December 1973.

5. R. Hofland, M. L. Lundquist, A. Ching, and J. S. Whitter, "Electron-Beam Irradiated Discharges for Initiating High-Pressure Pulsed Chemical Lasers," AIAA Paper No. 73-645.

6. S. C. Brown, Basic Data of Plasma Physics, 1966, Second Edition (The MIT Press).

7. S. Solimeno, "50 J Electrically Pulsed HF Chemical Laser," Fourth Conference on Chemical and Molecular Lasers, St. Louis, Missouri, October 1974.

8. R. Hofland, M. L. Lundquist, A. Ching, G. E. Thornton, and J. S. Whittier, "Dissociation Efficiency of Electron-Beam-Triggered Discharges for Initiating Atmospheric-Pressure H_2-F_2 Lasers," AIAA Paper No. 75-848.

9. P. Mahadevan and R. Hofland, "Absolute Cross Sections for Dissociative Electron Attachment to F_2," Aerospace Corp., to be published.

10. R. Hofland, A. Ching, M. L. Lundquist, and J. S. Whitter, "Atmospheric Pressure H_2-F_2 Laser Initiated by Electron-Beam Irradiated Discharge," Report No. SAMSO-TR-74-195, The Aerospace Corporation, July 1974.

11. A. Mandl, B. Kivel, and E. W. Evans, J. Chem. Phys., Vol. 53, 1970, p. 2363.